OXYGEN AND HYDROGEN ISOTOPIC ANALYSIS OF TOURMALINES BY SECONDARY ION MASS SPECTROMETRY

By

Jessica L. Whattam

A Thesis
Submitted to the Faculty of Graduate Studies of
The University of Manitoba
In Partial Fulfillment of the Requirements
For the Degree of

MASTER OF SCIENCE

Department of Geological Sciences
University of Manitoba
Winnipeg, Manitoba

Abstract

The O and H isotopic composition of minerals can provide valuable information on the source of the fluids and temperature of mineral precipitation. To obtain accurate isotopic measurements using SIMS, it is important to select chemically similar standards and samples to correct for both matrix effects and instrumental mass fractionation (IMF), collectively termed instrumental mass bias (IMB). For certain mineral groups (e.g. tourmalines), there are large variations in major element composition between species. This study uses three of these tourmaline species (schorl, dravite, and elbaite) to construct calibration curves to correct for IMB during SIMS analysis of O and H isotopes. I have applied my technique to analyses of tourmalines from the Wollaston Group, Athabasca region, Saskatchewan to test my method, and I have calculated the O and H isotopic composition of the fluids that formed these tourmalines.

Acknowledgements

This thesis could not have been completed without the wisdom, guidance, and funding from my professor Mostafa Fayek. I thank him for convincing me to move across the country and to learn about this interesting project. I also thank Frank Hawthorne for helping me to understand more about this complex group of minerals. David Quirt of AREVA Resources Canada Inc, thanks for the samples, help finding figures, and for being our resident chocolate milk connoisseur.

Thanks must also go to everyone in the Isotope Geology Lab group at the University of Manitoba. Ryan, Raven, Kevin, Brandi, Ian, Greg, Caitlin, Dan, Misuk, Yong Yong, Jincheng, thank all of you for being around for answers to my questions, coffee, help with the machines, help with figuring out my data, and for all round just being awesome people.

Thank you to all the grad students at U of M. You guys were paramount to me not going crazy while finishing this project. Especially my office mate Matt, Jemma and Lauren, I won't hold your soft rock preferences against you.

Externally to school, I have to thank my dog pack friends. Thanks for brining me out of science to unwind and play with all of your fluffy puppies and giving me an outlet for relaxing. Tara and Amber I will miss you both so much, thanks for letting me ramble about rocks even when it sounded like Greek.

Finally, I thank my family and friends back home in Nova Scotia. Your support throughout these past two years has been the reason I've made it this far. I've missed you all terribly and look forward to seeing you all in the near future.

- Jess.

Table of Contents

List of Tables

List of Figures

List of Copyrighted Material for which Permission was Obtained

Chapter 1: Introduction

The hydrogen and oxygen isotopic compositions of minerals, in combination with calculated mineral-fluid isotopic fractionation factors, have been used to determine the source of fluids, temperature, paleoclimatic conditions, duration of glacial events, and prehistoric trade routes of gem-quality minerals (Eiler et al., 1997; Sharp, 2007; Valley & Kita, 2009 and references therein). The oxygen isotopic compositions of most silicate and oxide minerals are often obtained from bulk powdered samples and the laser-fluorination method (Sharp, 1990) or the BrF_5 method (Clayton & Mayeda, 1963). Over the past two decades, secondary ion mass spectrometry (SIMS) has allowed *in situ* micro-analysis of oxygen isotope in silicates, oxides and carbonates with precision that rivals bulk conventional methods (Riciputi et al., 1998; Valley & Kita, 2009). Conventional bulk analytical methods (Vennemann and O'Neil, 1993; Duncan et al., 2014) are still preferred for hydrogen isotope analysis of minerals and rocks. However, there are several recent studies of hydrogen isotope analysis of minerals and volcanic glasses by SIMS (e.g., Hauri et al., 2006; Hull et al., 2008; Hull et al., 2014; Othmane et al., 2015).

The *in situ* capabilities of SIMS provide several advantages for analysis of oxygen and hydrogen isotopes in minerals. These advantages include simple sample preparation, and the capability of analysis of finely-zoned minerals and of multiple generations of minerals. However, complex instrument calibration methods are often required to obtain precise and accurate isotopic analysis by SIMS. Analysis of isotopes by SIMS requires that standards are used to calibrate for matrix effects and instrumental mass fractionation (IMF) (Adams et al., 1989; Hervig et al., 1992; Riciputi et al., 1998; Peacock & Hervig, 1999; Kasemann et al., 2001; Coakley et al., 2005; Valley & Kita, 2009). For the purpose of this thesis, I define IMF as isotopic fractionation occurring during SIMS analysis (e.g.: sputtering, ionization, transmission of secondary ions, and secondary ion detection), and matrix effects as the effects on the IMF

associated with the chemical composition of the sample. Collectively, IMF and matrix effects are referred to as "instrumental mass bias" (IMB; Riciputi et al., 1998).

1.1 Tourmaline

The tourmaline supergroup currently has 31 minerals with the very complex general formula $XY_3Z_6(T_6O_{18})(BO_3)_3V_3W$, where X = Ca, Na, K, or vacancy; Y = Li, Mg, Fe^{2+}, Mn^{2+}, Zn, Al, Cr^{3+}, V^{3+}, Fe^{2+}, Ti^{4+}, or vacancy; Z = Mg, Al, Fe^{3+}, Cr^{3+}, V^{3+}; T= Si, Al or B; B = B or vacancy; V = OH, or O; and W = OH, F or O (Henry et al., 2011). The nomenclature of tourmaline species is based on the occupancy of each site. Groupings are determined starting with the cation (or vacancy) of the X site, followed by the W site which controls the prefix of the species name, and then by the Y site. All tourmaline group minerals are cyclosilicate minerals. They often form tabular to prismatic crystals, however, acicular, massive, and radial habits of these minerals have also been found in nature (Henry & Dutrow, 1996; Hawthorne & Dirlam, 2011). Tourmaline is of interest to geologists for a variety of reasons. First, it is the largest geological sink for boron (B) (Henry and Dutrow, 1996; Hawthorne and Henry 1999; Jiang et al., 1999; Beurlen et al., 2011; Henry et al., 2011; Mercadier et al., 2012; Bast et al., 2014). Second, tourmaline is an important gem mineral with beautiful samples from around the world being mined for their wide array of colours (Zachariáš et al., 2005; Shabaga et al., 2010; Beurlen et al., 2011; Ludwig et al., 2011).

Tourmaline is also an indicator mineral for many economic mineral deposits, including uranium (Hoeve and Quirt, 1984; Kotzer & Kyser, 1995; Dipak et al., 2010; Mercadier et al., 2012; Reid et al., 2013), copper (Dipak et al., 2010; Hawthorne and Dirlam 2011; Trumbull et al., 2011; Baksheev et al., 2012) gold, lead, zinc, silver, tungsten, tin, iron, and REEs (Jiang et al., 1999; Henry & Brodtkorb, 2009; Dipak et al., 2010; Shabaga et al., 2010; Hawthorne &

Dirlam, 2011; Shuschevskaya et al., 2011; Trumbull et al., 2011; Baksheev et al, 2012). Toumaline occurs in all three rock types, but notably in granitic pegmatites (Jiang et al., 1999; Trumbull & Chaussidon, 1999; Zachariáš et al., 2005; Maloney et al., 2008; Shabaga et al., 2010; Beurlen et al., 2011; Hawthorne & Dirlam, 2011; Ludwig et al., 2011; Baksheev et al., 2012; Marks et al., 2013), metamorphic and metasomatic rocks (Henry & Dutrow, 1996; Bebout & Nakamura, 2003; Hawthorne & Dirlam, 2011; Henry & Dutrow 2012; Mercadier et al., 2012; Bast et al., 2014), and less commonly in sedimentary rocks as either detrital tourmaline or as diagenetic overprints (Henry & Dutrow, 1996; 2012). The common occurrence of tourmaline, and its resistance to changes in pressure and temperature make tourmaline an ideal recorder of the initial geochemical conditions of its host rock (Henry & Dutrow, 1996; Bebout & Nakamura, 2003; Maloney et al., 2008; Shabaga et al., 2010; Hawthorne & Dirlam 2011; Ludwig et al., 2011; Baksheev et al., 2012; Bast et al., 2014). In addition, combining hydrogen and oxygen isotopic analyses in tourmaline can lead to a better understanding of fluid source(s) responsible for forming the tourmaline and the ore deposits associated with tourmalines, such as the unconformity-type uranium deposits.

1.2 Purpose of this study

The overall goal of this study is to develop a methodology for measuring oxygen and hydrogen isotopes in tourmaline using SIMS. To achieve this goal, specific objectives are to i) select appropriate tourmaline calibration standards for oxygen and hydrogen isotopic analysis by SIMS, ii) determine the key factors (e.g., chemical composition) that most strongly affect instrumental mass bias, and iii) test the methodology on tourmalines from the Wollaston Group, East Athabasca region, Saskatchewan, Canada.

Chapter 2: Methodology

Eight tourmaline grains were obtained from Professor Frank Hawthorne from the University of Manitoba. They will henceforth be referred to by their sample ID or as "calibration samples". The tourmaline samples used in this study are elbaite, dravite, and schorl species which have identical chemical formulae with the exception of the cation occupying the Y-site of the species.

2.1 Electron Microprobe Analysis

The major element chemical compositions of the calibration samples were analyzed using the electron microprobe (EMP). Electron microprobe analysis was performed using a CAMECA SX100 electron microprobe at the University of Manitoba. For wavelength-dispersive spectrometry (WDS) analysis, CAMECA's Peak Sight software was used. In WDS mode, an accelerating voltage of 15 keV was used with a beam current of 20 nA and beam diameter of 10 μm. The following crystals and mineral standards were used: TAP: albite (Na); andalusite (Al) diopside (Si); LPET: diopside (Ca); orthoclase (K); sphene (Ti); LLIF: fayalite (Fe); spessartine (Mn); LTAP: riebeckite (F); olivine (Mg). Microprobe analysis of the samples from the Wollaston Group (referred to by their sample ID or as "application samples") also used the same instrument parameters. The results of the EMP analyses are presented in Section 3.1 (Table 1) and in Appendix A.

2.2 LA-ICP-MS

The electron microprobe is incapable of accurately measuring lithium (Li) concentrations. Therefore, a laser-ablation inductively coupled plasma mass-spectrometer (LA-ICP-MS) was used to measure the concentration of Li in each calibration sample. Measurements of Li were obtained using a Thermo Finnigan Element single-collector ICP-MS at the University

of Manitoba coupled with a New Wave 213nm laser-ablation system. The laser was operated with a fluence of 4 J/cm, a pulse frequency of 10 Hz and a beam size of 30 μm. Ablation was performed in spot mode with a total analytical time per spot of 100 s – 50 s of a gas blank and 50 s of ablation to increase accuracy and precision. Sample points were taken in a traverse across the grain to provide more representative sampling, and to be able to determine if any chemical zonation was present in the samples. The results of the LA-ICP-MS analyses are presented in Section 3.1 (Table 1) and in Appendix Bin Table 1.

2.3 Bulk Oxygen and Hydrogen Isotopic Analysis

Splits of the eight tourmaline calibration samples were crushed into a powder and analyzed for their $\delta^{18}O$ values using the BrF_5 method (Clayton & Mayeda, 1963) at Queen's University, Canada. δD values were obtained using a thermo-combustion elemental analyzer (TC/EA) coupled to a Thermo-Finnigan Delta^{Plus} XP continuous-flow isotope-ratio mass-spectrometer (CFRIMS) at the University of Manitoba. The values are reported in Table 2 and in Appendix C, and discussed in Sections 3.6 and 3.7. They represent the "true" $\delta^{18}O$ and δD values. These "true" values have been used to correct for IMB during SIMS isotopic analysis (Sections 3.6 and 3.7).

2.4 SIMS Analyses

Prior to SIMS analysis, grains of the eight calibration samples were cut perpendicular to the c-axis and mounted into SIMS pucks using Buehler Epo-Thin® epoxy and left to cure for ~24 hours. Once cured, the samples were polished (using both wet/dry sandpaper and diamond polishing paste) until the grains were flat and had smooth polished surfaces. The polished sample mounts were cleaned using an ultrasonic bath (10 min. per cycle using i) tap water and soap, ii) tap water, iii) distilled water, and iv) ethanol) to remove any residual polishing pastes.

Application samples were made into thin sections and then cut into circles to be put in the SIMS sample holder after undergoing the same cleansing protocols. All samples were sputter coated with gold for 30 seconds to produce a conductive sample surface and put into the SIMS airlock overnight to ensure a high vacuum. The average vacuum for δD analysis was on the order of 4.5 x 10^{-9} torr.

The isotopic ratios for $^{18}O/^{16}O$ were measured using a CAMECA ims 7f secondary ion mass spectrometer at the University of Manitoba (Winnipeg, Canada). A 1.3 nA beam of $^{133}Cs^{+}$ ions was used as the primary beam, and mass resolving power was set to 347 with a voltage offset set to +250 V to limit interferences. The sample-accelerating voltage was +10.5 kV and electrostatic analyzer in the secondary column was set to accept -9 kV. Using an ETP electron multiplier coupled with an ion-counting system, ions were detected with an overall deadtime of 28 ns. Total analytical time for O analysis was approximately 10 minutes. Oxygen isotopic data for the calibration samples are given in Table 3 in Section 3.3.

The hydrogen isotopic ratios (D/H) were measured using a CAMECA ims 7f secondary ion mass spectrometer at the University of Manitoba (Winnipeg, Canada). A ~50 nA beam of O^{-} ions accelerated to 12.5 keV was used as the primary beam, with a -50 V offset applied to minimize isobaric interferences. Entrance and exit slits were narrowed to maintain a mass resolving power of 800 and ensure flat top peaks. The sample-accelerating voltage was 12.5 kV and the electrostatic analyzer in the secondary column was set to accept +10 kV. Using an ETP AF133H electron multiplier coupled with an ion-counting system, ions of D and H were detected counting H for 1 second and D for 5 seconds. Magnet settling time was 0.5 s and the overall deadtime for the EM was 21 ns. Total analytical time was ~ 15 minutes using 90 cycles. Hydrogen isotopic data for the calibration samples are given in Table 4.

2.4.1 SIMS Data Manipulation and Calculations

The second objective in this study is to test the method created, and determine if the fluids responsible for forming the tourmaline could be sourced correctly using the isotopic composition of the tourmaline. To do this calibration curves were constructed using the calibration samples to correct the raw SIMS data for IMB (See Figures 2.1, 2.2). Using the equation of the calibration curves, the appropriate fractionation factor (α_{inst}) for each tourmaline can be calculated and applied to resolve the IMB associated with the concentration of Fe or Mg in each application sample. Once the α_{inst} is calculated for each application sample, that value is used to calculate the "true" isotopic value of the sample given by equation (1). In this equation, Rmeas is the ratio of $^{18}O/^{16}O$ or D/H obtained from the SIMS.

$$\alpha inst = Rmeas/Rtrue \quad \textbf{(1)}$$

Once the "true" ratios of the application samples were determined they were then converted into permil (‰) notation relative to VSMOW in order to calculate the values of the fluid. Temperature estimates of 700°C were used (see chapter 4) and the isotopic composition of the fluid was calculated using the equations by Zheng (1993; equation (2)) for oxygen and Jibao and Yaqian (1997; equation (3)) for hydrogen.

$$\boldsymbol{\delta^{18}OTur - \delta^{18}OFlu = 4.21\left(\frac{10^6}{T^2}\right) + (-6.99)\left(\frac{10^3}{T}\right) + 2.14} \quad \textbf{(2)}$$

$$\boldsymbol{\delta DTur - \delta DFlu = -27.9\left(\frac{10^6}{T^2}\right) + 0\left(\frac{10^3}{T}\right) + 2.3} \quad \textbf{(3)}$$

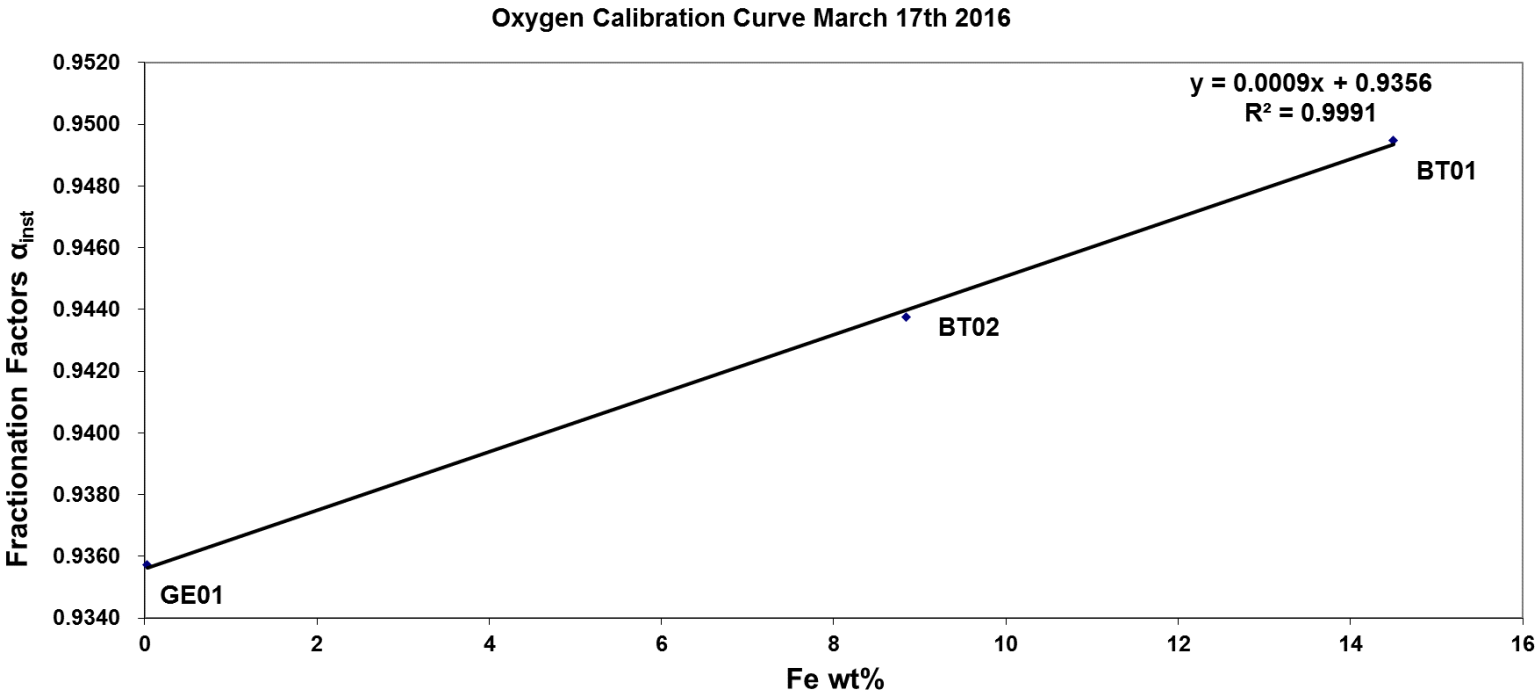

Figure 2.1 Oxygen calibration curve used for correcting IMB for application samples

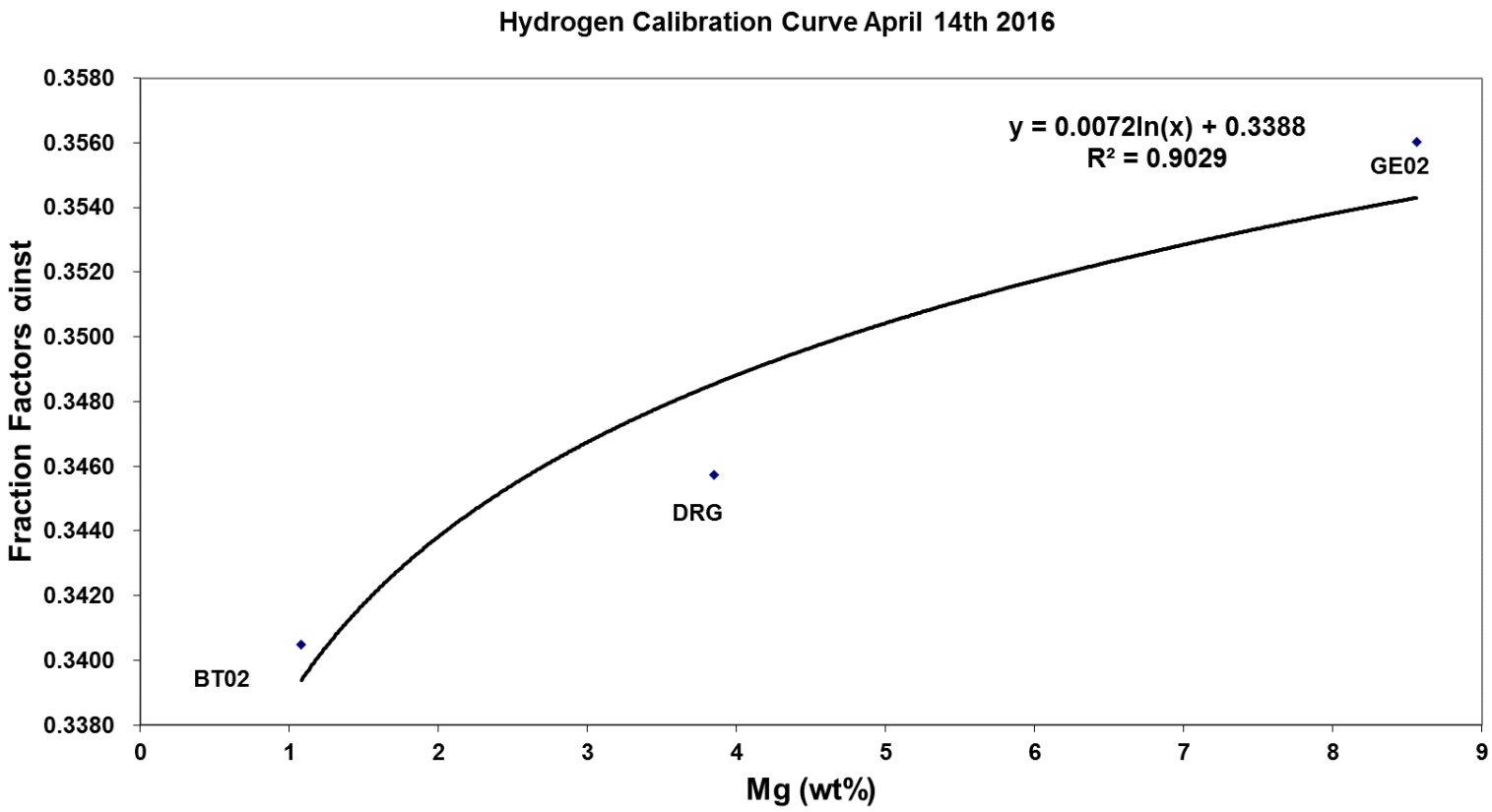

Figure 2.2 Hydrogen Calibration curve used to correct IMB for application samples

Chapter 3: Results

3.1 Electron Microprobe and LA-ICP-MS Results

Selected results for Al, Fe, and Mg from the EMP analyses and Li from the LA-ICP-MS analyses are presented in Table 1. All the data from the EMP analyses are presented in Appendix A, while all Li and B data from the LA-ICP-MS analyses are presented in Appendix B.

Table 1. Li, B, Al, Fe and Mg concetrations in tourmaline calibration samples

Sample	Li (ppm)*	B (wt%)*	Al (wt%)	Fe (wt%)	Mg (wt%)
BT01	343	3.41	16.30	14.50	0.06
BT02	440	3.42	18.50	8.84	1.08
CE01	299	4.06	23.00	0.01	0.00
DRG	17.3	3.44	13.20	2.87	3.85
GE01	8.43	3.50	15.80	0.03	8.00
GE02	4.55	3.48	14.90	0.03	8.56
PE01	10982	3.88	22.30	0.08	0.00
PE02	11194	3.47	22.10	0.02	0.00

* Li and B data were obtained using LA-ICP-MS

3.2 Bulk Oxygen and Hydrogen Isotopic Analysis Results

The results from the bulk oxygen and hydrogen isotopic analyses are presented in Table 2 and all the data are presented in Appendix C.

Table 2. "True" $\delta^{18}O$ and δD values for tourmaline calibration samples

Sample	Yield (μmol/mg CO_2)	$\delta^{18}O$ vs VSMOW (‰)	Yield (% H_2O)	δD vs VSMOW (‰)
BT01	15.1	9.5	2.8	-88
BT02	15.3	6.8	3.3	-64
CE01	16.1	14.1	3.5	-99
DRG	15.6	13.4	3.2	-47
GE01	15.9	19.7	3.9	-50
GE02	15.9	19.7	3.9	-50
PE01	14.7	12.3	3.7	-105
PE02	17.0	10.8	3.5	-83

3.3 SIMS Oxygen and Hydrogen Isotopic Analysis Results

Oxygen and hydrogen isotopic data for the calibration samples are presented in Tables 3 and 4, including all errors associated with the SIMS analyses. These errors include within spot error, spot to spot reproducibility (within session error), and total error.

Table 3. SIMS oxygen isotope data for eight tourmaline grains used as calibration samples

Sample	End Member	$^{18}O/^{16}O_{meas}$	Within Spot Error (1σ)[1]	Within Session Error (1σ)[2]	Total Error (2σ)[3]	α_{inst}[4]	IMF (‰)[5]
BT01	Schorl	1.9144	0.6	0.7	0.7	0.9457	-54.3
BT02	Schorl	1.8954	0.6	0.8	0.7	0.9389	-61.1
CE01	Elbaite	1.8924	0.6	0.8	0.7	0.9306	-69.4
DRG	Dravite	1.8972	0.6	0.7	0.7	0.9337	-66.4
GE01	Elbaite	1.9053	1.2	1.2	1.2	0.9318	-68.2
GE02	Elbaite	1.9029	1.0	1.1	1.1	0.9306	-69.4
PE01	Elbaite	1.8880	0.7	0.8	0.8	0.9301	-69.9
PE02	Elbaite	1.8869	0.8	0.9	0.9	0.9310	-69.1

1. Poisson countint statistics from SIMS

2. Standard deviation of samples anayzed given by $SD = \sqrt{\Sigma(Xi-X)^2/(n-1)}$

3. Total error defined by $2\sigma = \sqrt{[(Spt^2)*0.8+(WiSpt^2)*0.2]}$

4. α_{inst} given as R_{meas}/R_{true}

5. $IMF = (R_{meas}/R_{true}-1)*1000$

Table 4. SIMS hydrogen isotope data for eight tourmaline grains used as samples

Sample	End Member	Session	D/H_{meas}	Within Spot Error (1σ)[1]	Within Session Error (1σ)[2]	Total Error (2σ)[3]	α_{inst}[4]	IMF (‰)[5]
BT01	Schorl	June, 2015	5.3517E-05	13	1.7	6.0	0.3643	-636
BT02	Schorl	June, 2015	4.8026E-05	11	1.8	5.2	0.3297	-659
CE01	Elbaite	June, 2015	4.9515E-05	12	4.0	6.4	0.3528	-647
DRG	Dravite	June, 2015	5.0187E-05	11	2.1	5.3	0.3381	-662
GE01	Elbaite	June, 2015	5.0179E-05	11	3.9	6.0	0.3391	-661
GE02	Elbaite	June, 2015	5.0703E-05	12	3.6	6.3	0.3550	-657
PE01	Elbaite	June, 2015	4.7525E-05	13	3.2	6.5	0.3409	-659
PE02	Elbaite	June, 2015	5.0095E-05	12	2.1	5.7	0.3507	-671
BT01	Schorl	November, 2015	5.4406E-05	12	3.4	6.2	0.3700	-630
BT02	Schorl	November, 2015	5.0416E-05	13	1.1	5.9	0.3436	-664
CE01	Elbaite	November, 2015	5.1595E-05	12	3.2	6.1	0.3655	-634
DRG	Dravite	November, 2015	5.3061E-05	11	1.6	5.1	0.3534	-655
GE01	Elbaite	November, 2015	5.2908E-05	11	3.2	5.7	0.3516	-656
GE02	Elbaite	November, 2015	5.3386E-05	12	2.8	5.9	0.3800	-653
PE01	Elbaite	November, 2015	4.7399E-05	13	6.1	8.0	0.3301	-670
PE02	Elbaite	November, 2015	5.3283E-05	12	1.7	5.6	0.3795	-629

1. Poisson countint statistics from SIMS

2. Standard deviation of samples anayzed given by $SD = \sqrt{\Sigma(Xi-X)^2/(n-1)}$

3. Total error defined by $2\sigma = \sqrt{[(Spt^2)*0.8+(WiSpt^2)*0.2]}$

4. α_{inst} given as R_{meas}/R_{true}

5. IMF = $(R_{meas}/R_{true}-1)*1000$

3.4 Chemical Composition of Calibration Samples

The eight calibration samples used for this study were originally identified and labelled by private mineral collectors. Samples BT-01 and BT-02 were both previously identified as schorls with a chemical formula of $NaFe^{2+}{}_3Al_6Si_6O_{18}(BO_3)_3(OH)_3OH$ (Henry et al., 2011). These two samples have higher Fe contents than the rest of the calibration samples. Samples CE-01, PE-01, and PE-02 were all identified as elbaite species with the mineral composition of $Na(Li_{1.5}Al_{1.5})Al_6Si_6O_{18}(BO_3)_3(OH)_3OH$ (Henry et al., 2001) with trace Fe (<1 wt%). Samples GE-01, and GE-02 were also previously identified as elbaite species of tourmaline. However, they contain ≥8 wt% Mg, and therefore these samples are now reclassified as solid solution dravite-elbaites. Sample DRG (dravite - $NaMg_3Al_6Si_6O_{18}(BO_3)_3(OH)_3OH$ (Henry et al., 2001)),

contains higher than expected Fe (2.87 wt%). Pure dravite does not usually contain Fe, however a solid solution exists between many of the tourmaline endmembers (Henry & Dutrow, 1996; Hawthorne & Dirlam, 2010) including dravite-schorl. Figure 3.1 is a plot of the calibration samples as functions of their concentrations of Mg and Fe in wt%, which separates the pure species from those that may be of solid solution species of tourmalines.

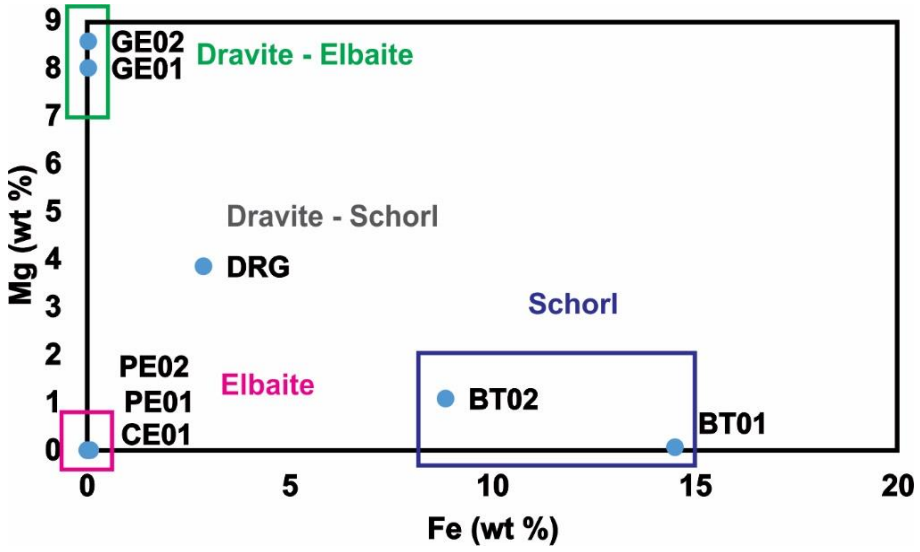

Figure 3.1 Calibration samples plotted as functions of their wt% Fe and Mg concentrations

3.5 Calibration Samples - Suitability as SIMS standards

Based on the SIMS isotopic analysis, BT-01, BT-02, CE-01, DRG, PE-01 and PE-02 are sufficiently homogenous (where the spot-to-spot reproducibility, also known as "within session error" (Table 3), is <1‰) at the micrometer scale that they can be used as calibration standards for SIMS oxygen isotope analysis,-. Samples GE-01 and GE-02 have a higher spot-to-spot reproducibility (1.0-1.2‰).

With respect to hydrogen homogeneity, all calibration samples (with the exception of PE-01) had spot-to-spot reproducibility (Table 4) of <4‰. Therefore, seven of the eight samples

(BT-01, BT-02, CE-01, DRG, GE-01, GE-02, and PE-02) are sufficiently isotopically homogenous to be used as calibration standards for SIMS hydrogen isotopic analysis.

A test was conducted to examine the hypothesis that one or more of the calibration samples could be treated as a standard and used to correct the SIMS values of all of the other calibration samples (Tables 5 & 6). However, it was determined that individual tourmaline species cannot be used to correct the SIMS O and H isotopic data of all species and that matrix matching to the mineral group type (tourmaline) was not sufficient for SIMS isotopic analysis of tourmaline. These results indicate that there is likely some major-element component within tourmaline that has a larger control on IMB for oxygen and hydrogen isotope analysis by SIMS.

Table 5. $\delta^{18}O$ (‰) values for each sample corrected using different grains as standards.

Sample	"True" Value	BT01	BT02	CE01	DRG	GE01	GE02	PE01	PE02
BT01	**9.5**	-	17.1	26.1	22.8	24.8	26.1	26.7	25.8
BT02	**6.8**	-0.5	-	15.7	12.4	14.4	15.7	16.2	15.3
CE01	**14.1**	-2.1	5.2	-	10.8	12.8	14.1	14.6	13.7
DRG	**13.4**	0.5	7.7	16.7	-	15.4	16.7	17.2	16.3
GE01	**19.7**	4.7	12.2	21.0	17.7	-	21.0	21.6	20.7
GE02	**19.7**	3.5	10.8	19.7	16.4	18.4	-	20.3	19.4
PE01	**12.3**	-4.4	3.3	11.8	8.5	10.5	11.7	-	11.4
PE02	**10.8**	-5.0	16.2	11.1	7.8	9.9	11.1	11.7	-

"True" values were obtained using CFRIMS and all samples are reported in permil notation relative to VSMOW

Table 6. δD(‰) values for each sample corrected using different grains as standards.

Sample	"True" Value	BT01	BT02	CE01	DRG	GE01	GE02	PE01	PE02
BT01	**-88**	-	-55	-75	-20	-10	-45	-9	-17
BT02	**-64**	-157	-	-41	-90	-98	-147	-100	-123
CE01	**-99**	-130	-27	-	-60	-68	-119	-70	-94
DRG	**-47**	-118	-20	4	-	-56	-107	-57	-81
GE01	**-50**	-112	-14	11	-41	-	-102	-52	-76
GE02	**-50**	-109	-10	15	-37	-46	-	-48	-72
PE01	**-105**	-162	-69	-46	-95	-104	-152	-	-128
PE02	**-83**	-119	-22	-3	-49	-58	-109	-59	-

"True" values were obtained using a TC/EA coupled with CFRIMS and all samples are reported in permil notation relative to VSMOW

3.6 Oxygen and Hydrogen isotopes and IMB

The three different tourmaline species used are similar in chemical composition with the exception of the cations that fill the Y site in the tourmaline crystal structure. The calculated IMB values for both oxygen (Figure 3.2) and hydrogen (Figure 3.3) for each sample was plotted against their Li, Mg, and Fe concentrations, to determine if there is a relationship between IMB and any major Y-site element concentrations.

3.6.1 Oxygen Isotopes

In Figure 3.2A, there is no correlation observed between Li content and the IMB for oxygen – in the low-Li samples. In Figure 3.2B, there is a strong linear correlation between Fe content and the IMB, with a R^2 value of 0.9889. In Figure 3.2C, the IMB for all 8 samples was plotted against the respective Mg concentrations. In Figure 3.2D, only samples containing ≥ 0.05 wt % Mg are plotted, and they show a negative logarithmic correlation between the IMB and Mg concentration, with a R^2 value of 0.9287. The relationship between IMB and Mg concentration (Figure 3.2D) is also related to the Fe concentration (Figure. 3.2B) because Mg^{2+} can substitute for Fe^{2+}. Aluminum was also evaluated to determine if there was a relationship between Al and IMB, it is not depicted in the figures because no relationship exists. Therefore,

when measuring O isotopes in tourmaline by SIMS, it is important to know the concentrations of both Fe in the calibration sample and Fe in the application samples so that the appropriate calibration curves can be applied to the application sample data. For samples not containing Fe (eg. calibration samples PE01, PE02, CE01), no IMB calibration is needed for O isotope analysis (Figure 3.2 A, C as no correlation exists.

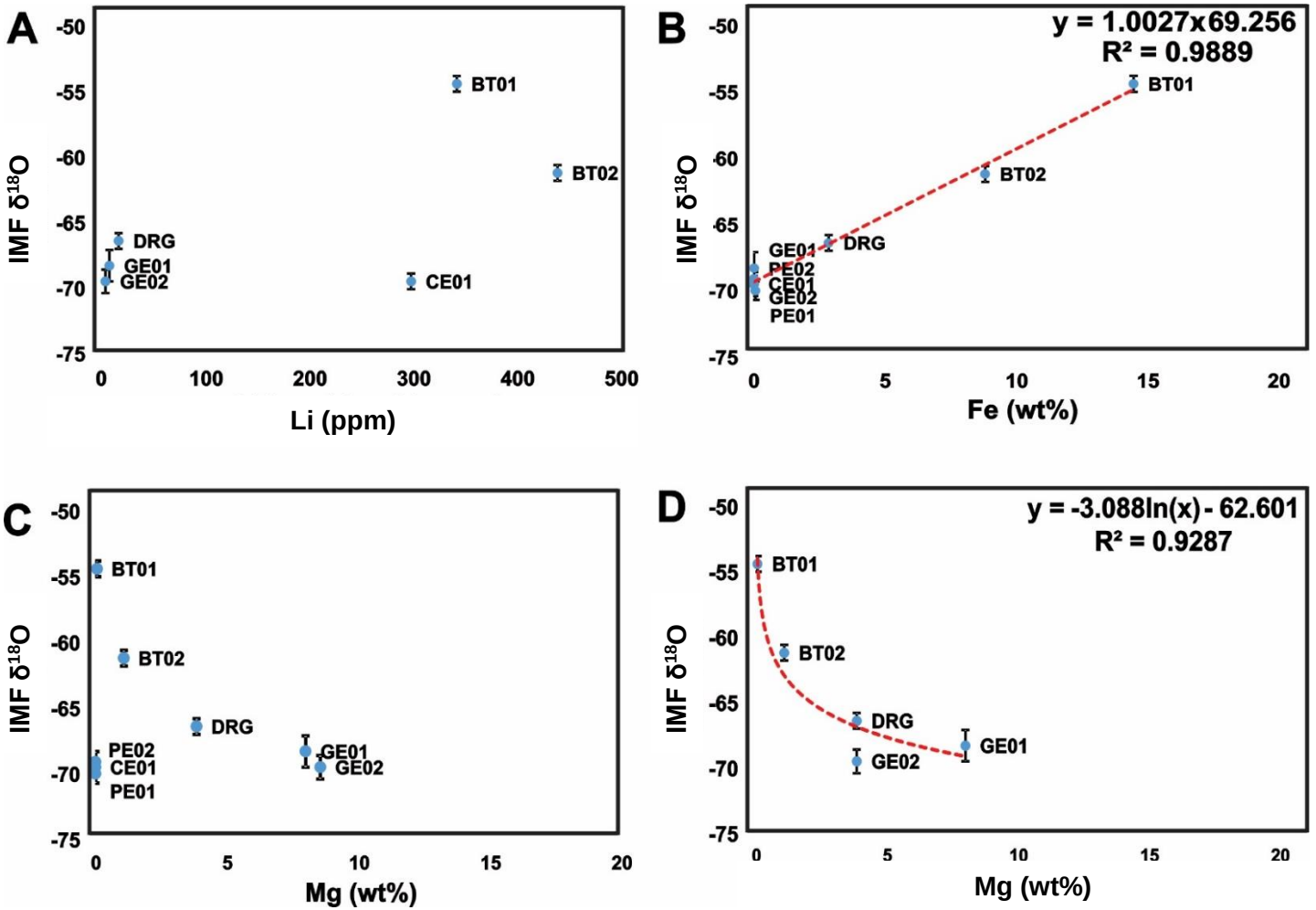

Figure 3.2: Relationships between Y site elements and IMB for $\delta^{18}O$ values. A: low concentration (Li < 500 ppm) Li samples vs IMB. B: Fe vs IMB. C: Mg vs IMB. D: Mg vs IMB for samples with > 0.05 wt% Mg

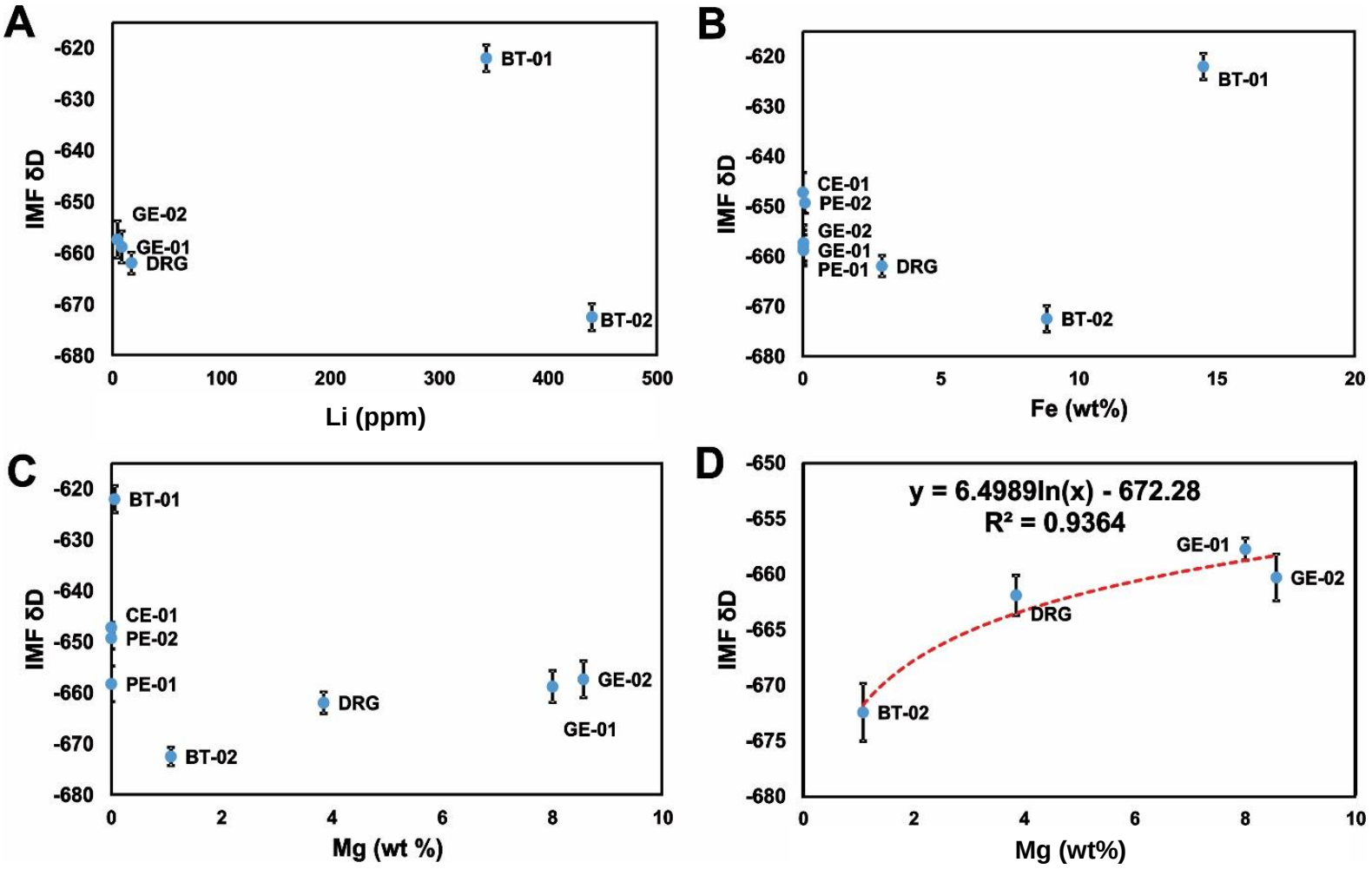

Figure 3.3: Relationships between Y site elements and IMB for δD values. A: low concentration (Li < 500 ppm) Li samples vs IMB. B: Fe vs IMB. C: Mg vs IMB. D: Mg vs IMB samples with > 0.05 wt% Mg

3.6.2 Hydrogen Isotopes and IMB

Similar to the oxygen isotopes, the IMB for hydrogen isotope analyses were plotted against the concentration of elements at the Y-site. There are no correlations between Li and Fe concentrations, and the IMB values (Figures 3.3A, B), there is also no relationship between IMB and Al concentration even though it is not depicted in the figures below. There is, however, a positive correlation between Mg concentrations ≥1 wt % and IMB, with a R^2 of 0.9364 (Figure 3.3D). The strong relationship between Mg concentration and the IMB for hydrogen, and the lack of such a relationship for Fe in tourmalines was surprising because some minerals, such as turquoise (Hull et al., 2008; Hull et al., 2014; Othmane et al., 2015), and volcanic glasses (Hauri et al., 2002; Hauri et al., 2006), show a relationship between IMB and Fe concentration. Therefore, when analyzing the hydrogen isotopic composition of tourmaline, it is important to know the concentration of Mg in tourmaline samples prior to SIMS analysis so that the correct calibration curves can be applied to the raw hydrogen isotopic data from the SIMS analysis.

3.7 Crystallographic Orientation Effects

Another important parameter to evaluate when analyzing isotopic compositions of minerals using SIMS is the possibility of orientation effects caused by analyzing grains that are in one crystallographic orientation versus analyzing those same grains in another crystallographic orientation. Orientation effects during SIMS analysis have been reported for carbonates (Rollion-Bard & Marin-Carbonne 2011), muscovite (Deloule et al 1991), brucite (Riciputi et al., 1997), phengite (Ottolini et al., 2002), magnetite (Lyon et al., 1998; Huberty et al., 2010), rutile (Schmitt & Zack, 2012; Taylor et al., 2012), and baddeleyite (Wingate & Compston, 2000; Li et al., 2010). In these studies, crystal orientation effects were observed to

produce up to ~10‰ variation in IMB. In this study four crystals were cut and mounted in two different crystallographic orientations: parallel to the *c-axis* and perpendicular to the *c-axis*. Crystal orientation effects were not observed for SIMS oxygen isotope analysis in tourmaline Crystals analyzed parallel to the *c-axis* of the tourmaline produced results that were within analytical error of results from those crystals analyzed perpendicular to the c-axis, and therefore, orientation effects for oxygen are negligible and do not appear in Table 7.

With respect to hydrogen, orientation effects were observed in two of the four crystals analyzed (Table 7). The ~15‰ variation represents the maximum difference between two perpendicular orientations. It is not yet fully understood why some tourmalines show this orientation effect with respect to hydrogen and others do not. However, for the purpose of obtaining the most precise and accurate SIMS data, it is recommended to have tourmaline standards mounted in multiple crystallographic orientations.

Table 7. SIMS data of hydrogen isotopes for crystallographically oriented samples

Sample	Session and Orientation	Mass Bias (‰)	Δorientation
BT01	Aug ∥ c-axis	-691	
	Aug ⊥ c-axis	-677	14
	Nov ∥ c-axis	-629	
	Nov ⊥ c-axis	-616	13
PE01	Aug ∥ c-axis	-722	
	Aug ⊥ c-axis	-709	13
	Nov ∥ c-axis	-672	
	Nov ⊥ c-axis	-658	14
PE02	Aug ∥ c-axis	-688	
	Aug ⊥ c-axis	-692	-4
	Nov ∥ c-axis	-631	
	Nov ⊥ c-axis	-633	-2
CE01	Nov ∥ c-axis	-639	
	Nov ⊥ c-axis	-640	-1

∥ c-axis: parallel to c-axis of the grain

⊥ c-axis: perpendicular to the c-axis of the grain

Chapter 4: Application of SIMS O and H isotopic correction methodology – Application Samples

To test the methodology described in this thesis, I applied my technique to two geologically well-constrained anatectic and metamorphic tourmaline samples from the Wollaston Group of the Athabasca region of northern Saskatchewan (Figures. 4.1, 4.2). I used my data to calculate the oxygen and hydrogen isotopic composition of fluids that formed the tourmalines. The samples analyzed were selected from barren locales (Figures. 4.1, 4.2, 4.3, 4.4, 4.5) and therefore, the fluids associated with these samples are expected to have a different hydrogen and oxygen isotopic composition, compared to mineralizing fluids associated with unconformity-related uranium deposits from the Athabasca Basin.

4.1 Geologic Setting

4.1.1 Regional Geology

The samples collected for the purpose of testing this new SIMS methodology are from the Wolly/McClean Lake area of the eastern Athabasca Basin of northern Saskatchewan (Fig. 5.1), approximately 750 km north of Saskatoon and 400 km north of La Ronge. The Athabasca Basin is an approximately 100 000 km^2 intra-cratonic basin located in northwestern Saskatchewan and extending slightly into North Eastern Alberta (Fayek & Kyser, 1997; Ramaekers et al 2007; Laverett et al., 2006; Sheahan et al., 2016). The crystalline basement below the Athabasca Basin is comprised of highly deformed medium- to high-grade metamorphic Archean and Paleoproterozoic gneisses and comprises portions of both the Rae and the Hearne sub-provinces of the Western Churchill Structural Province of the Canadian Shield. In the study area, the basement is composed of two domains within the Hearne sub-province. The Wollaston Domain contains Paleoproterozoic Wollaston Group metasedimentary rocks of amphibolite to lower-granulite facies and the Mudjatik Domain is dominantly upper amphibolite

facies orthogneisses. The Wollaston Domain is a distinctly northeast-trending fold-thrust belt composed of the Wollaston Group metasediments overlying Archean granitoid gneisses, while the Mudjatik Domain is a northeast-trending, shear-bounded belt consisting mainly of Archean felsic gneisses (Annesley et al., 2005). Both domains have undergone complex polyphase deformation and metamorphism during the Trans-Hudson Orogeny , including intrusion of anatectic igneous bodies. The Wollaston–Mudjatik Transition Zone forms a 1-5 km wide transition from the strongly strike-slip Wollaston Domain to the more interference-folded Mudjatik Domain. These basement rocks are intruded by Wollaston Group anatectic pegmatites (Annesley et al., 2005, Campbell, 2007; Tourigny et al., 2007; McKeough et al., 2013) that are generally biotite-bearing with occasional sulfides, but locally contain abundant tourmaline rather than biotite.

The Athabasca Basin is filled by the Athabasca Group sandstone that is dominantly comprised of fluvial deposits that unconformably overlie the basement rocks. These strata presently have a maximum thickness of approximately 1500 m and were deposited approximately 1750-1700 Ma during post-Hudsonian tectonic relaxation. (Fayek & Kyser, 1997; Annesley et al., 2005; Laverret et al., 2006; Ramaekers et al., 2007, Sheahan et al., 2016).

4.1.2 Local Geology

The Wolly/McClean Lake project area of the Athabasca Basin is located on the eastern margin of the Athabasca Basin (Figs. 4.1, 4.2, 4.3) and straddles the Wollaston-Mudjatik Transition Zone. In the McClean Lake area, the sub-Athabasca basement geology is characterized by a "dome and basin" setting where, in plan view (Fig. 4.3), large Archean granitoid "domes" alternate with stratigraphically-overlying Paleoproterozoic Wollaston Group metasedimentary rocks. The McClean, Sue, and Jeb deposits are situated between two Archean

basement domes (McClean Lake dome and Torwalt dome) and are associated with linear graphitic pelitic gneiss units.

The Athabasca Group sandstone ranges in thickness from 10 to 200 m over the McClean Lake property and comprises only the lowest Manitou Falls Formation: the MFb (Bird) Member (Campbell, 2007; Ramaekers et al., 2007; Tourigny et al, 2007).

Tourmaline samples for this study were collected by AREVA Resources Ltd. (Table 8; Figure 4.0 and are from a Wollaston pegmatite (sample R237), and from a Wollaston tourmalinite (sample SL81).

Table 8. Application sample description list. Information collected by AREVA Resources Ltd.

Sample ID	Depth (m)		Description	Location
	From	To		
R-237/159.8	159.8	159.9	fresh Wollaston tourmaline pegmatite	McClean Lake project, Jeb South area
SL-81/109.7	109.7	109.9	relatively fresh Wollaston tourmalinite	Wolly project

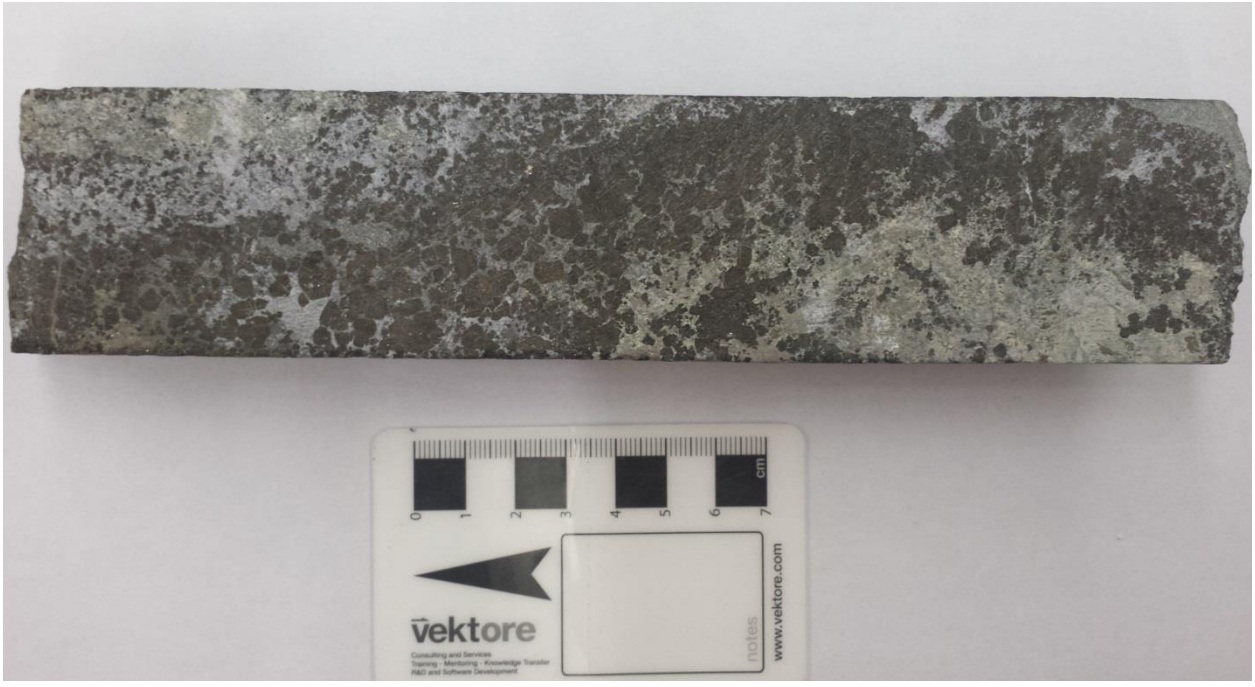

Figure 4.0 - Core photo of Sample SL-81

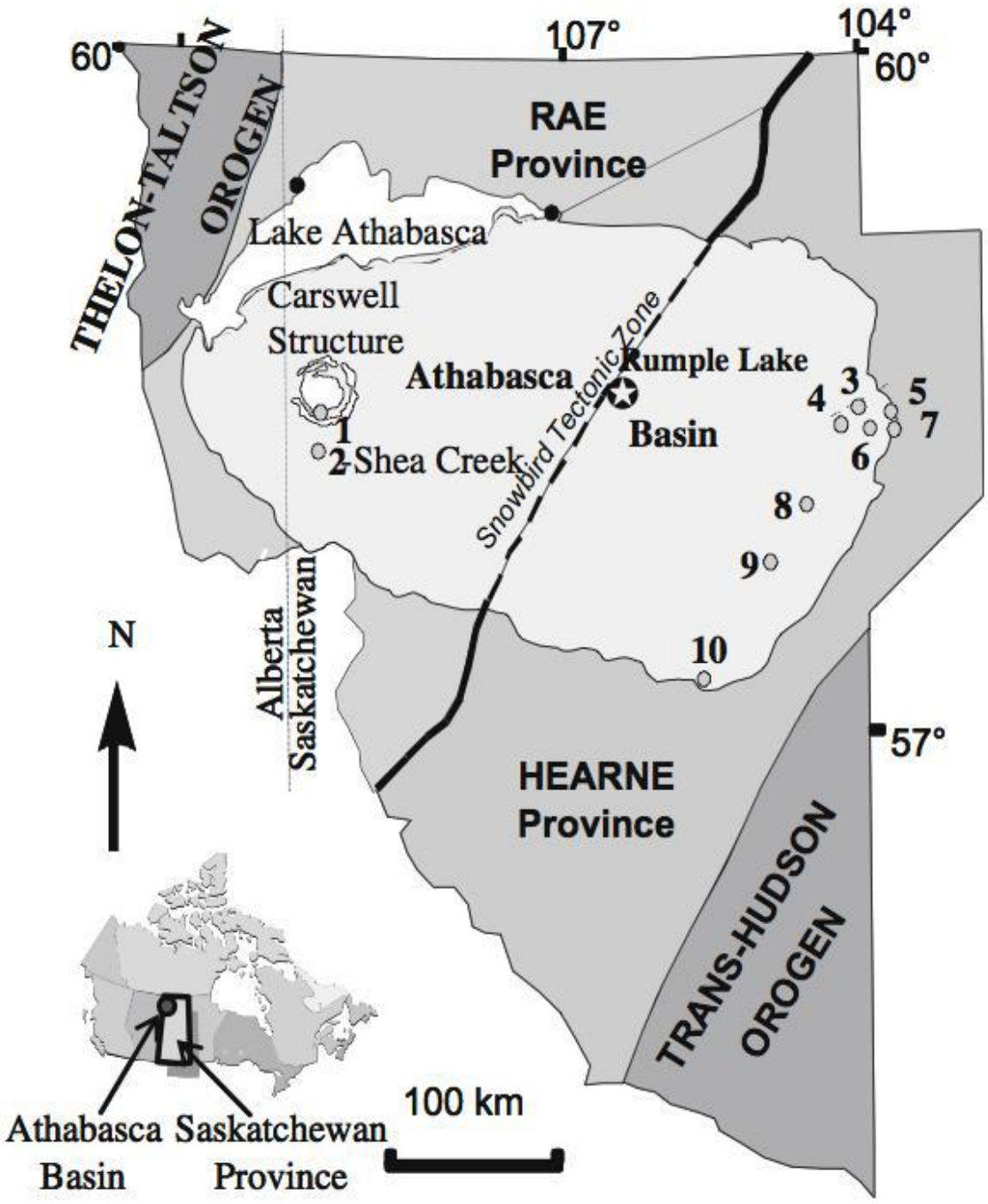

Figure 4.1: Location map of the Athabasca Basin (northern Saskatchewan, Canada). The Major U deposits are: Cluff Lake (1), Shea Creek (2), Dawn Lake (3), Midwest(4), Collins Bay (5), McClean Lake and Sue (6), Rabbit Lake (7), Cigar Lake (8), McArthur River (9), and Key Lake (10). From Laverett et al., 2006. Used with permission from the Clay and Clay Minerals Society

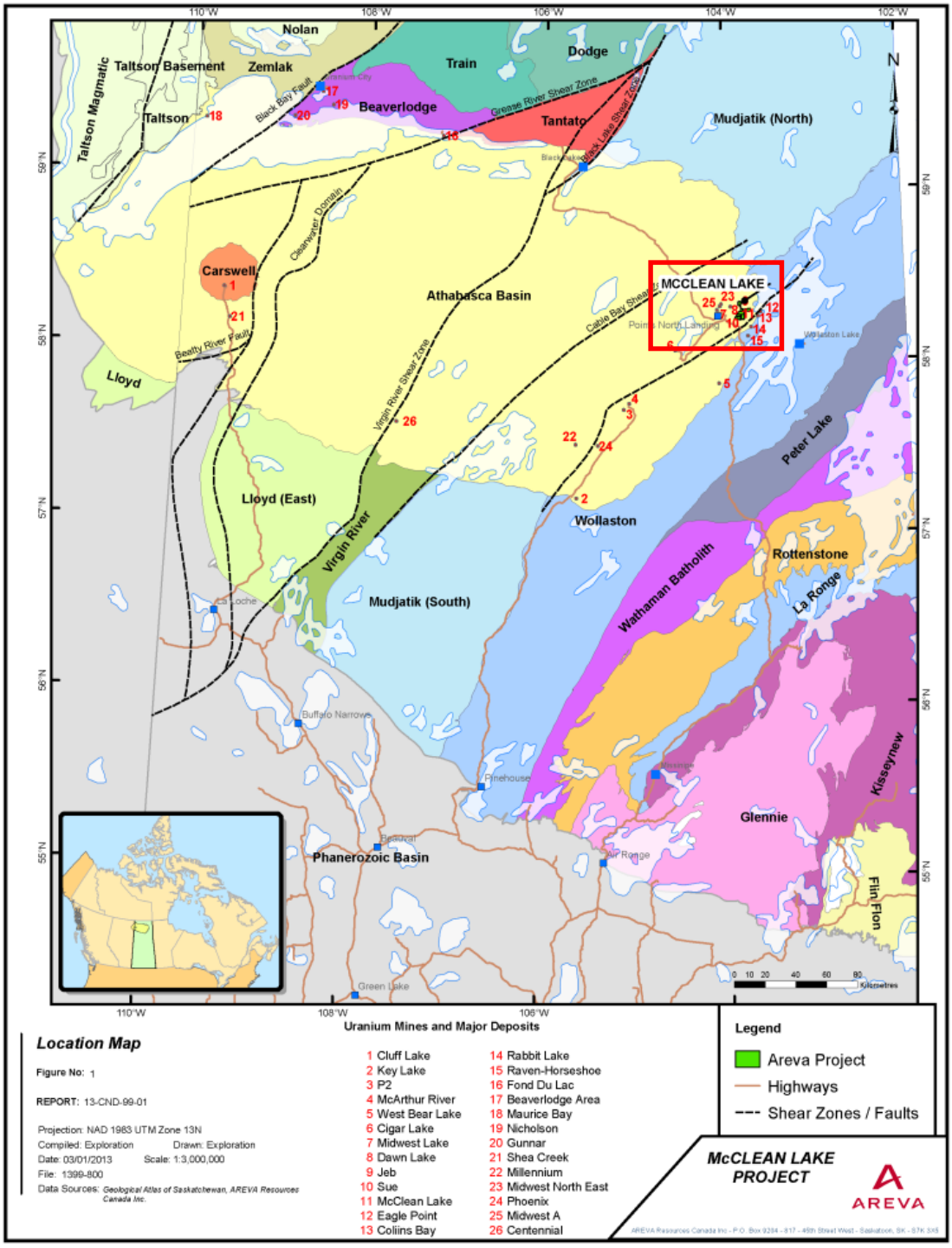

Figure 4.2 Plan map showing location of the Athabasca Basin and the Wolly/McClean project area. Used with permission from AREVA Resources Canada (2015).

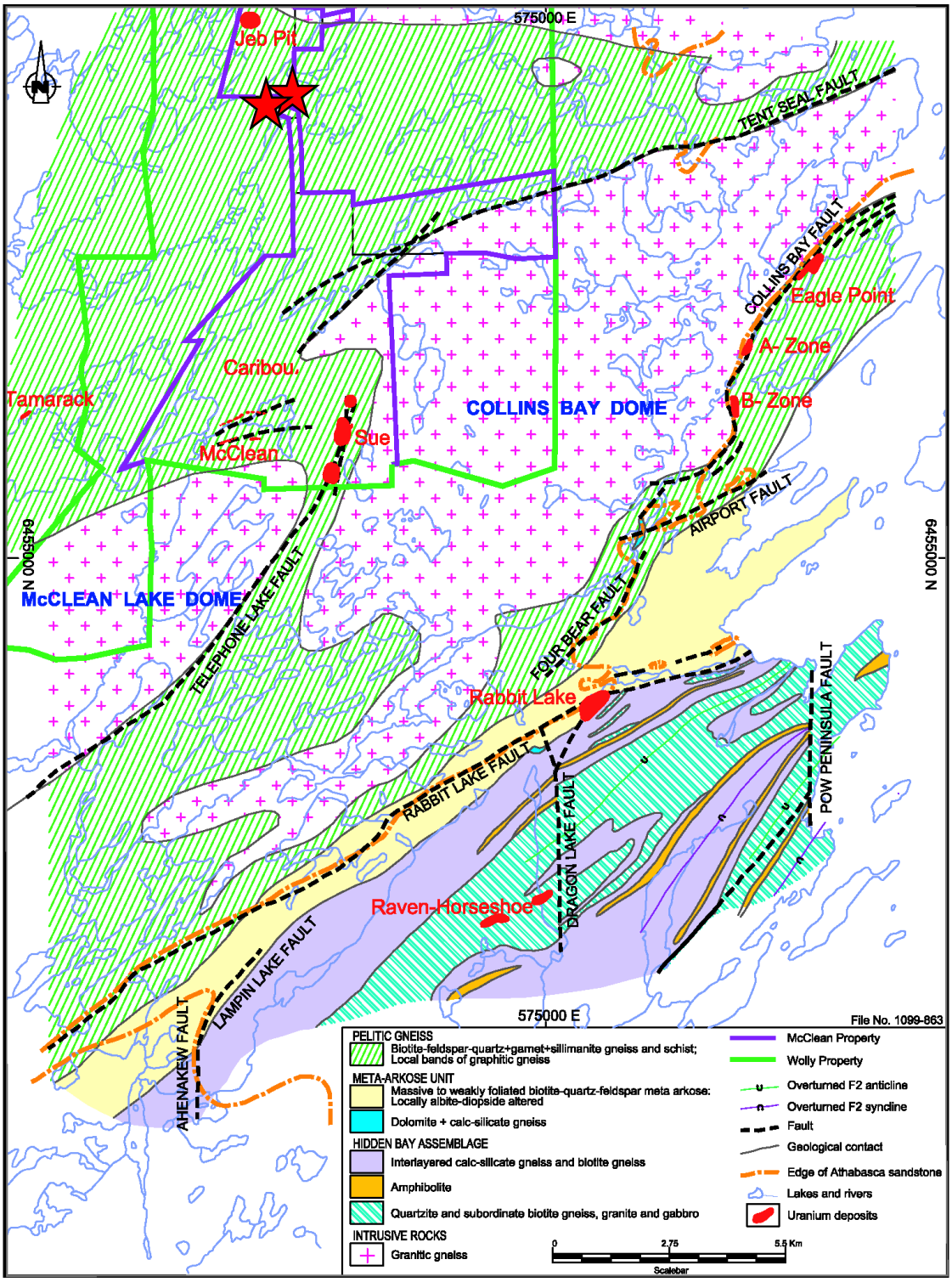

Figure 4.3 Plan map showing the geology of the McClean Lake area. Sample locations are denoted by stars. Used with permission from AREVA Resources Canada (2015).

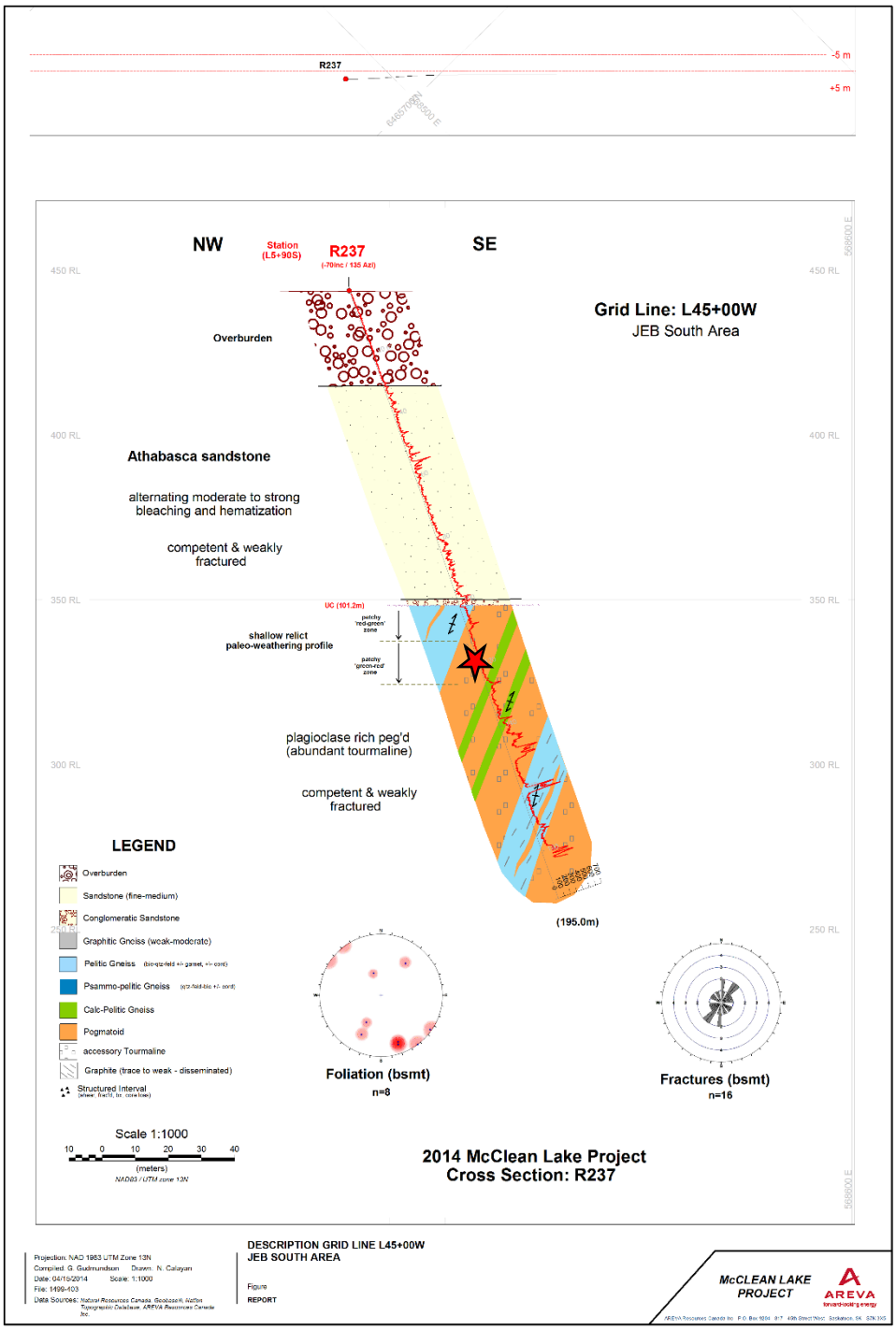

Figure 4.4: Cross-section of the McClean Lake Project Area (drill hole R237, with location of sample R237 denoted with a star). Used with permission from AREVA Resources Inc.

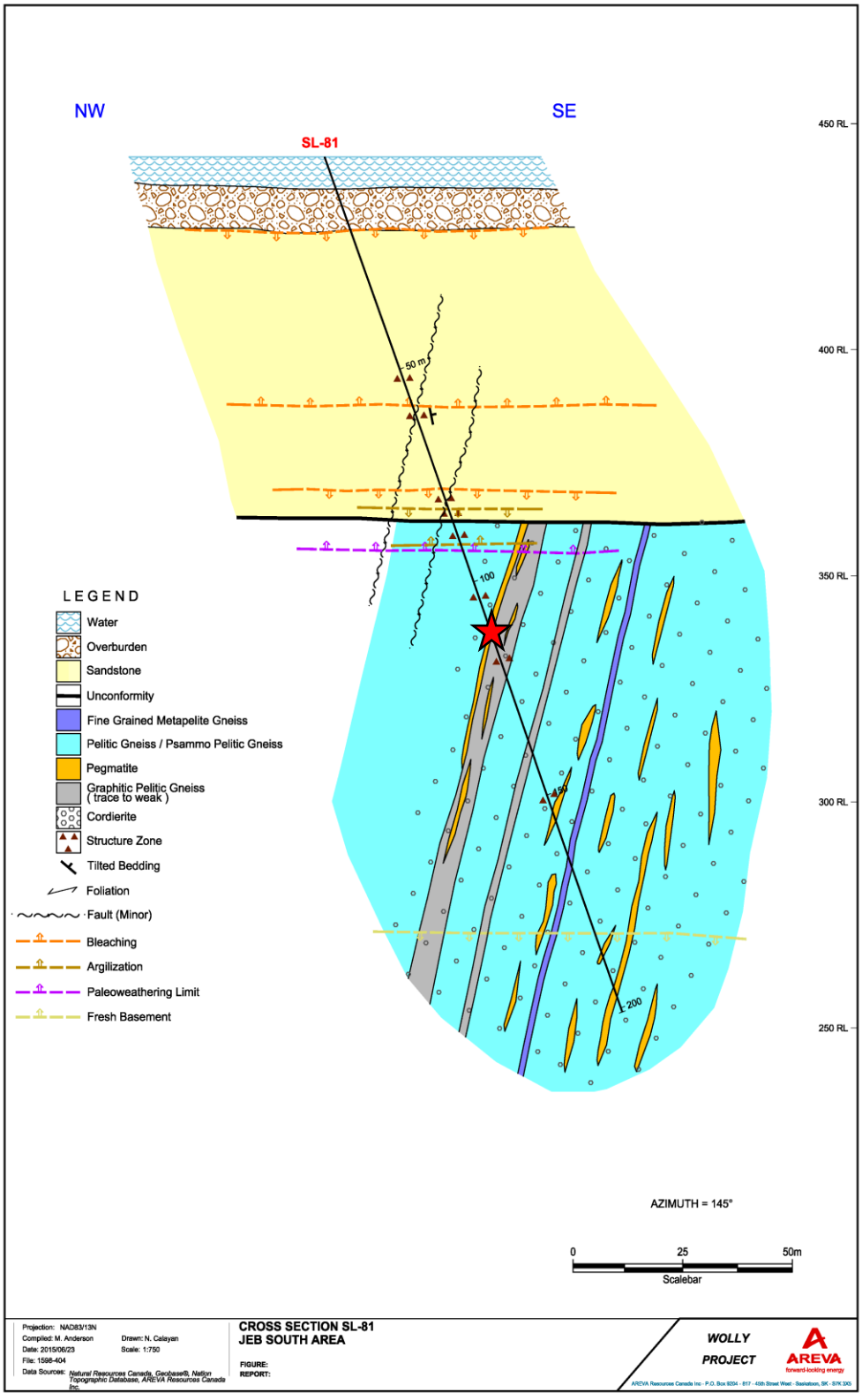

Figure 4.5: Cross-section of the Wolly Project Area (drill hole SL-81, with location of sample SL81 denoted with a star). Used with permission from AREVA Resources Inc.

4.2 Isotopic composition of application samples

The SIMS isotopic data for the Wollaston tourmaline samples are reported in Tables 9 and 10 for oxygen and hydrogen, respectively. The corrected $\delta^{18}O$ values obtained for the metamorphic tourmalines (in tourmalinite) are in the range of 12.2 to 19.2 ‰ and the tourmalines from the Wollaston pegmatite have oxygen values ranging from 12.7 to 13.8 ‰. Corrected hydrogen δD isotopic values of the tourmalinite tourmalines are between -114 and -59 ‰ and are between -138 and -119 ‰ for the pegmatite tourmalines. These values were used to calculate the isotopic composition of the fluids responsible for forming the tourmalines.

The oxygen isotopic composition of the fluids that formed these tourmalines were calculated using the fractionation-factor equation of Zheng (1993). The hydrogen isotopic composition of the fluid was calculated using the fractionation-factor equation of Jibao & Yaqin (1997). Calculations were made using a temperature estimate of 700°C for the anatectic igneous pegmatite samples because tourmaline often occurs as a late magmatic mineral in granites and granitic pegmatites (Henry & Guidotti, 1985; Pivec et al., 1998; Keller et al., 1999; Tindle et al., 2002; Longfellow & Swanson, 2011). A temperature of 700°C for the metasedimentary tourmalinite samples was used because the metasedimentary units in the Wolloston Domain were subjected to upper amphibolite-facies metamorphism (Annesley et al., 2005, Campbell, 2007; Tourigny et al., 2007; McKeough et al., 2013), which ranges from 500°C to 700°C (Winter, 2010).

The tourmalinites (samples SL81TL and SL81BR) formed from a fluid with $\delta^{18}O$ composition between 13.1‰ to 19.8‰ (Table 9) and with δD composition between -92‰ to -32‰ (Table 10), indicating a metamorphic fluid origin (Sharp, 2007). The tourmalines in the Wollaston pegmatite formed from a fluid with $\delta^{18}O$ composition between 12.7‰ to 13.8‰

(Table 9) and with δD composition between -138‰ to -119‰ (Table 10) indicating that anatectic (metamorphic) fluids may have interacted with organic-rich waters (Fig 4.6; Sharp, 2007).

The results of my study of the samples from the Wollaston Group indicate that anatectic pegmatite tourmaline and metamorphic tourmalines from the Athabasca region equilibrated with fluids that are isotopically distinct from fluids that are associated with uranium mineralization (Fayek & Kyser, 1997; Kotzer & Kyser, 1995; Annesley et al., 2005; Campbell, 2007; Raemakers et al., 2007; Tourigny et al., 2007; McKeough et al., 2013; Richard et al., 2013).

Table 9: Measured mineral $\delta^{18}O$ and calculated $\delta^{18}O$ values for fluids in equilibrium with tourmaline.

		Tourmaline Mineral Values				Fluid Values	
Sample	Origin of Tourmaline	Fe(wt%)	FF	$\delta^{18}O_{VSMOW}$ (‰)	1σ	$\delta^{18}O_{VSMOW}$ (‰)	1σ
SL81TL-DR4	Tourmalinite	4.98	0.9407	15.0	1.2	15.6	1.2
SL81TL-DR5	Tourmalinite	4.99	0.9411	13.5	1.2	14.1	1.2
SL81TL DR6	Tourmalinite	5.39	0.9415	19.2	1.2	19.8	1.2
SL81TL- DR7	Tourmalinite	4.98	0.9411	14.4	1.2	15.0	1.2
SL81TL - DR8	Tourmalinite	5.21	0.9413	14.8	1.2	15.4	1.2
SL81TL-DR9	Tourmalinite	4.97	0.9411	15.0	1.2	15.6	1.2
SL81TL-DR11	Tourmalinite	5.38	0.9414	13.0	1.3	13.6	1.3
SL81TL-DR12	Tourmalinite	5.38	0.9414	12.2	1.2	13.8	1.2
SL81TL-DR14	Tourmalinite	5.38	0.9414	14.6	1.1	15.2	1.1
SL81BR	Tourmalinite	5.39	0.9415	12.5	1.2	13.1	1.2
R237-DR6	Tourmaline Pegmatite	7.57	0.9434	12.8	1.3	13.4	1.3
R237-DR7	Tourmaline Pegmatite	7.56	0.9434	12.7	1.2	13.3	1.2
R237-DR8	Tourmaline Pegmatite	7.15	0.9430	13.8	1.1	14.4	1.1

Table 10: Measured mineral δD and calculated δD values for fluids in equilibrium with tourmaline.

		Tourmaline Mineral Values				Fluid Values	
Sample	Origin of Tourmaline	Mg (wt%)	FF	δD_{VSMOW} (‰)	1σ	δD_{VSMOW} (‰)	1σ
SL81TL-DR4	Tourmalinite	4.08	0.3418	-59	9.9	-31.8	9.9
SL81TL-DR5	Tourmalinite	3.99	0.3417	-92	11.4	-64.8	11.4
SL81TL DR6	Tourmalinite	3.76	0.3416	-119	10.9	-91.8	10.9
SL81TL- DR7	Tourmalinite	4.07	0.3417	-83	10.5	-55.8	10.5
SL81TL - DR8	Tourmalinite	3.88	0.3416	-72	10.7	-44.8	10.7
SL81TL-DR9	Tourmalinite	4.00	0.3417	-61	1.2	-33.8	1.2
SL81TL-DR11	Tourmalinite	3.79	0.3416	-114	10.9	-86.8	10.9
SL81TL-DR12	Tourmalinite	4.03	0.3417	-78	10.7	-50.8	10.7
SL81TL-DR14	Tourmalinite	3.79	0.3416	-94	10.9	-66.8	10.9
SL81BR	Tourmalinite	3.99	0.3433	-94	12	-66.8	12
R237-DR6	Tourmaline Pegmatite	2.33	0.3416	-119	12.8	-91.8	12.8
R237-DR7	Tourmaline Pegmatite	2.25	0.3415	-138	12	-110.8	12
R237-DR8	Tourmaline Pegmatite	2.68	0.3421	-120	12	-92.8	12

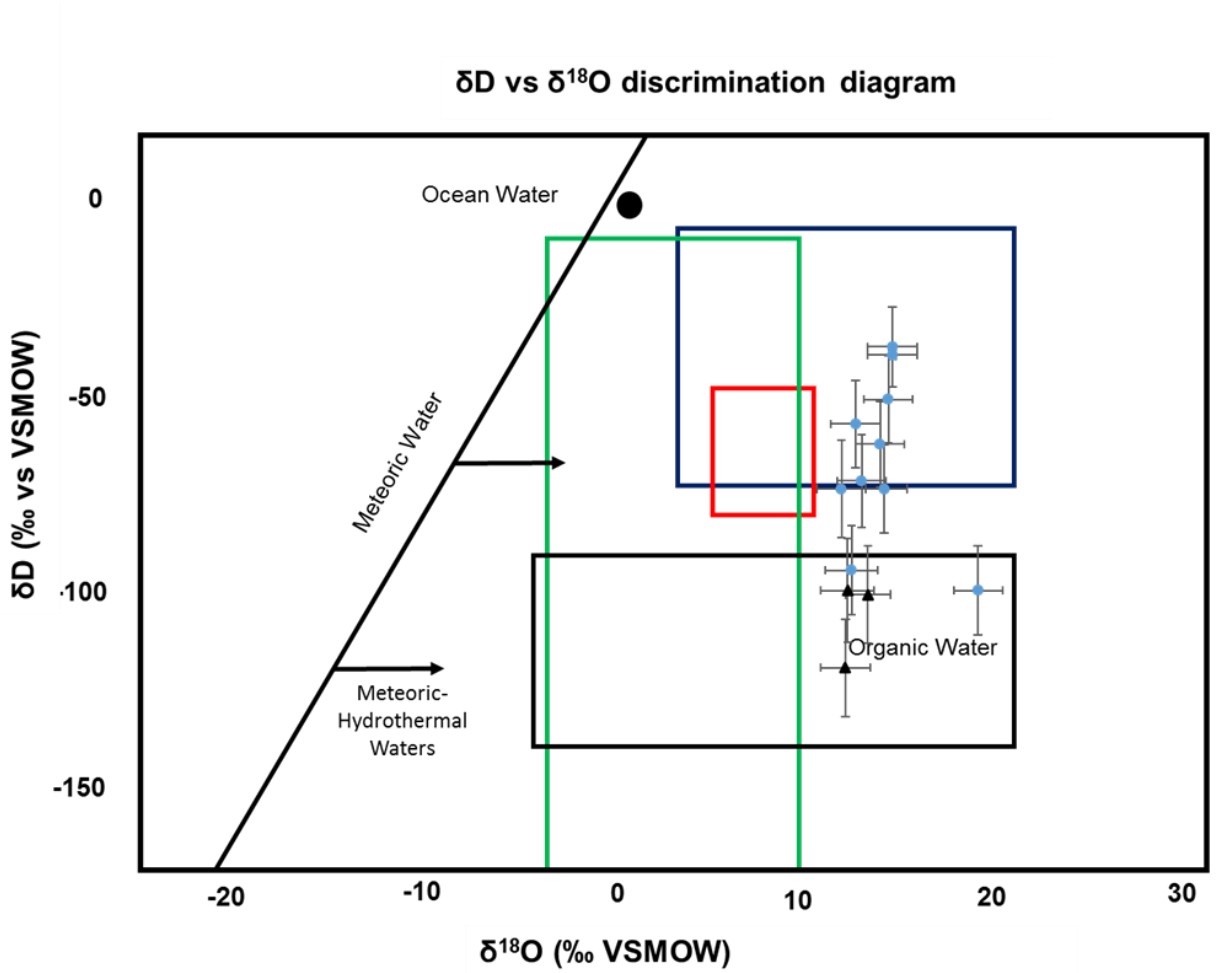

Figure 4.6 Oxygen and hydrogen isotopic composition of different fluid reservoirs (diagram after Sharp, 2007). The blue box represents the metamorphic fluids field, the red box represents the primary igneous fluids field and the green box represents the fluids associated with uranium mineralization from the Athabasca Basin: (Kotzer & Kyser, 1993; Kyser et al., 2000; Alexandre et al., 2005; Cloutier et al., 2010; and Sheahan et al. 2016.). The blue circles represent fluids in equilibrium with metamorphic tourmalines and the black triangles are fluids associated with pegmatite tourmalines from the Athabasca Basin. Modified from Sharp, 2007.

Chapter 5: Conclusion

The oxygen and hydrogen isotopic compositions of eight tourmaline grains (calibration samples) were obtained using SIMS to select the most isotopically homogenous grains for potential use as SIMS standards for O and H isotopic analyses using SIMS. Electron microprobe and LA-ICP-MS methods were used to obtain the major element compositions of these grains to determine the effects of chemical composition on IMB. The results lead to four main conclusions:

1. All potential standard samples, (with the exception of samples GE-01 and GE-02), are sufficiently isotopically homogenous at the micrometer scale with respect to their oxygen isotopic composition. Therefore, they can be used as analytical standards for oxygen isotope analysis by SIMS. With respect to hydrogen, nearly all potential standard samples (with the exception of PE02), can be used as analytical standards.
2. Fe has a large effect on IMB for oxygen isotope analysis and Mg has a large effect on hydrogen isotope IMB. Therefore, specific tourmaline species should only be used to correct raw isotopic SIMS data for the same species (or at the very least contain similar concentrations of Fe and Mg, respectively). Alternatively, calibration curves can be used to correct for IMB, using several standards with a range of Fe and Mg contents.
3. The crystallographic orientation effect has the potential to cause additional errors of up to15‰. It is recommended to have standards mounted in multiple crystallographic orientations to allow evaluation of this potential analytical issue. It is still not clear why some tourmalines are affected by the orientation effect and not others.
4. When this method was applied to metamorphic tourmalines from the Wollaston Group in the Eastern Athabasca region of Saskatchewan, the calculated isotopic composition of the fluids that formed these tourmalines mostly plotted in the metamorphic field, which

shows that my method can be used to determine the isotopic composition of fluids associated with tourmalines found in various geological settings.

References

Adams, F., Micheiels, F., Moens, M., and Van Epsen, P. 1989. Secondary-ion mass spectrometery as a quantitative microanalytical technique. Analytica Chimica Acta. 216: 25-55.

Annesley, I.R., Madore, C., and Portella, P., 2005, Geology and thermotectonic evolution of the western margin of the Trans-Hudson Orogen: evidence from the eastern sub-Athabasca basement, Saskatchewan, Canadian Journal of Earth Sciences, v. 42, p. 573-597.

Bast, R., Scherer, E.E., Mezger, K., Austrheim, H., Ludwig, T., Marschall, H.R., Putnis, A., and Löwen, K. 2014. Boron isotopes in tourmaline as a tracer of metasomatic processes in the Bamble sector of Southern Norway. Contributions in Mineralogy and Petrology. 168: 1069-1090.

Baksheev, I.A., Yu Prokof'ev, V., Zaraisky, G.P., Chitalin, A.F., Yapaskurt, V.O., Nikolaev, Y.N., Tikhomirov, P.L., Nagornaya, E.V., Rogacheva, L.I., Gorelikova, N.V., and Kononov, O.V. 2012. Tourmaline as a prospecting guide for porphyry-style deposits. European Journal of Mineralogy. 24: 957-979.

Bebout, G.E., and Nakamura, E. 2003. Record in metamorphic tourmalines of subduction-zone devolatilization and boron cycling. Geology. 31(5): 407-410.

Beurlen, H., Moura, O.J.M., Soares, D.R., Da Silva, M.R.R., and Rhede, D. 2011. Geochemical and geological controls on the genesis of gem-quality "Paraíba Tourmaline" in granitic pegmatites from northeastern Brazil. Canadian Mineralogist. 49: 277-300.

Campbell, J.E., 2007. Quaternary geology of the eastern Athabasca Basin, Saskatchewan. , *in* Jefferson, C.W. and Delaney, G., eds., EXTECH IV: Geology and uranium exploration technology of the Proterozoic Athabasca Basin, Saskatchewan and Alberta, Geological Survey of Canada, Bulletin 588: 211-228.

Card, C.D., Pană, D., Portella, P., Thomas, D.J., and Annesley, I.R., 2007, New insights into the geological history of the basement rocks to the southwestern Athabasca Basin, Saskatchewan and Alberta, Geological Survey of Canada Bulletin, v. 4, issue 18, p. 119-133.

Clayton, R.N., and Mayeda, T.K. 1963. The use of bromine pentafluoride in the extraction of oxygen from oxides and silicate for isotopic analyses. Geochimica et Cosmochimica Acta, 27 (1): 43-52.

Coakley, K. J., Simons, D.S., Leifer, A.M. 2005. Secondary ion mass spectrometry measurements of isotopic ratios: correction for time varying count rate. International Journal of Mass Spectrometry. 240: 107-120.

Deloule, E., France-Lanord, C., and Albarède, F. 1991. D/H analysis of minerals by ion microprobe. In: H.P Taylor Jr., J.R., O'Neil, and I.R. Kaplan, EDS., A tribute to Samuel Epstein no. 3. The Geochemical Society, Special Publication: 53-62.

Dipak, C.P., Trumbull, R.B., Wiedenbeck, M. 2010. Chemical and boron isotope compositions of tourmaline from the Jaduguda U(-Cu-Fe) deposit, Singhbhum shear zone, India: Implications for the sources and evolution of mineralizing fluids. Chemical Geology. 277: 245-260.

Duncan, R.J., Buick, I.S., Kobayashi, K., Wilde, A.R., 2014. Chemical and stable isotope characteristics of syn-tectonic tourmaline from the Western fold belt, Mount Isa inlier, Queensland, Australia. Chemical Geology, 381: 131-143.

Eiler, J.M., Graham, C., Valley, J.W., 1997. SIMS analyses of oxygen isotopes: matrix effects in common minerals and glasses. Chemical Geology 138(4): 221-244.

Fayek, M. and Kyser, T.K., 1997, Characterization of multiple fluid-flow events and rare-earth-element mobility associated with formation of unconformity-type uranium deposits in the Athabasca Basin, Saskatchewan, The Canadian Mineralogist, v. 35, p. 627-658.

Hauri, E., Wang, J., Dixon, J.E., King, P.L., Mandeville, C., and Newman, S. 2002. SIMS investigations of volatiles in volcanic glasses, 1: calibration, sensitivity and comparisons with FTIR. Chemical Geology 183: 99– 114

Hauri, E.H., Shaw, A.M., Wang, J., Dixon, J.E., King, P.L., and Mandeville, C., 2006. Matrix effects in hydrogen isotope analysis of silicate glasses by SIMS. Chemical Geology. 235: 352-365.

Hawthorne, F.C., Dirlam, D.M. 2011. Tourmaline the indicator mineral: from atomic arrangement to Viking navigation. Elements. 7: 307-312.

Hawthorne, F.C., and Henry, D.J., 1999. Classification of the minerals of the tourmaline group. European Journal of Mineraology. 11: 201-215.

Henry, D.J., and Brodtkorb, M.K. 2009. Mineral chemistry and chemical zoning in tourmalines, Pampa del Tamboreo, San Luis, Argentina. Journal of South American Earth Sciences 28: 132-141.

Henry, D.J., and Dutrow, B.L. 1996. Metamorphic tourmaline and its petrologic applications. In L.M. Anovitz and E.S.Grew, Eds., Boron: Mineralogy, Petrology and Geochemistry, 33: 503-557. Reviews in Mineralogy, Mineralogical Society of America. Chantilly, Virginia.

Henry, D.J., and Guidotti, C.V. 1985. Tourmaline as a petrogenetic indicator mineral: an example from the staurolite-grade metapelites of NW Maine. American Mineralogist. 70: 1-15.

Henry, D.J., Novák, M., Hawthorne, F.C., Ertl, A., Dutrow, B.L., Uher, P., and Pezzotta, F. 2011. Nomenclature of the tourmaline-supergroup minerals. American Mineralogist. 96: 895-913.

Hervig, R.L., Williams, P., Thomas, R.M., Schauer, S.N., and Steele, I.M. 1992. Microanalysis of oxygen isotopes in insulators by secondary ion mass spectrometry. International Journal of Mass Spectrometry and Ion Processes. 120: 45-63.

Hoeve, J., and Quirt D. 1984. Mineralization and host-rock alteration in relation to clay mineral diagenesis and evolution of the middle-Proterozoic, Athabasca Basin, northern Saskatchewan, Canada. Saskatchewan Research Council, SRC Technical Report 187, 187 p.

Huberty, J.M., Kita, N.T., Kozdon, R., Heck, P.R., Fournelle, J.H., Michael, J.S., Xu, H., Valley, J.W. 2010. Crystal orientation effects of $\delta^{18}O$ for magnetite and hematite by SIMS. Chemical Geology. 276 (3):269-283

Hull, S., Fayek, M., Mathien, F.J., Shelley, P., and Durand, K.R., 2008. A new approach to determining the geological provenance of turquoise artifacts using hydrogen and copper stable isotopes. Journal of Archeological Science. 35 (5):1355-1369.

Hull, S., Fayek, M., Mathien, F.K., and Roberts, H., 2014. Turquoise trade of the ancestral puebloan: Chaco and beyond. Journal of Archeological Science. 45: 187-195.

Jiang, S-Y., Palmer, M.R., Slack, J.F., and Shaw, D.R. 1999. Boron isotope systematics of tourmaline formation in the Sullivan Pb-Zn-Ag deposit, British Columbia, Canada. Chemical Geology. 158: 131-144.

Jibao, G., and Yaqian Q. 1997. Hydrogen isotope fractionation and hydrogen diffusion in the tourmaline-water system. Geochimica et Cosmochimica Acta. 64: 4679-4688.

Kasemann, S., Meixner, A., Ricgikk, A., Vennemann, T., Rosner, M., Schmitt, K., and Wiedenbeck, M. 2001. Boron and oxygen isotope compositions of certified reference

materials NIST SRM 610/612 and reference materials, JB-2 and JR-2. Journal of Geostandards and Geoanalysis. 25 (2): 405-416.
Kotzer, T.G. and Kyser, T.K. 1995. Petrogenesis of the Proterozoic Athabasca Basin, northern - Saskatchewan, Canada, and its relation to diagenesis, hydrothermal uranium mineralization and paleohydrogeology. Chemical Geology. 120: 45-89.
Laverret, E., Patirer Mas, P., Beaufort, D., Kister, P., Quirt, D., Bruneton, P., and Clauer, N. 2006. Mineralogy and geochemistry of the host-rock alterations associated with the Shea Creek unconformity-type uranium deposits (Athabasca Basin, Saskatchewan, Canada). Part 1: Spatial variation of illite properties. Clay and Clay Minerals. 54 (3): 275-294.
Li, X-H., Liu, Y., Li, Q-L., Guo, C-H., Chamberlain, K.R. 2009. Precise U-Pb and Pb-PB dating of phanerozoic baddeleyite by SIMS with oxygen flooding technique. Journal of Analytical Atomic Spectrometry. 25 (7):1107-1113.
Longfellow, K.M. and Swanson, S.E. 2011. Skeletal tourmaline, undercooling and crystallization history of the Stone Mountain granite, Georgia, U.S.A. Canadian Mineralogist. 49 (1): 341-357.
Ludwig, T., Marschall, H.R., Pogdge von Stranimann, P.A.E., Shabaga, B.M., Fayek, M., and Hawthorne, F.C., 2011. A secondary ion mass spectrometry (SIMS) re-evaluation of B and Li isotopic compositions of Cu-bearing elbaite from three global localities. Mineralogical Magazine. 75 (4): 2485-2494.
Maloney, J.S., Nabelek, P.I., Sirbescu, M-L. C., and Halama, R. 2008. Lithium and its isotopes in tourmaline as indicators of the crystallization process in the San Diego County pegmatites, California, USA. European Journal of Mineralogy. 20: 905-916.
Marks, M.A.W., Marschall, H.R., Schühle, P., Guth, A., Wenzel, T., Jacob, D.E., Barth, M., and Markl, G. 2013. Trace element systematics of tourmaline in pegmatitic and hydrothermal systems from the Variscan Schwarzwald (Germany): The importance of major element compositon, sector zoning and fluid or melt compositon. Chemical Geology. 344: 73-90.
McKeough, M.A., Lentz, D.R., McFarlane, C. R. M., Brown, J. 2013. Geology and evolution of pegmatite-hosted U-Th ± REE-Y-Nb mineralization, Kulyk, Eagle, and Karin Lakes Region, Wollaston Domain, northern Saskatchewan, Canada: examples of the dual role of extreme fractionation and hybridization processes. Journal of Geosciences. 58: 321-346.
Mercadier, J., Richard, A., and Cathelineau, M. 2012. Boron- and magnesium-rich marine brines at the origin of giant unconformity-related uranium deposits: δ11B evidence from Mg-tourmalines. Geology. 40: 231-234.
Othmane, G., Hull, S., Fayek, M., Rouxel, O., Geagea, M.L., and Kyser, T.K., 2015. Hydrogen and copper isotope analysis of turquoise by SIMS: calibration and matrix effects. Chemical Geology. 395: 41-49.
Ottolini, L., Cámara, F., Hawthorne, F.C., Stirling, J. 2002. SIMS matrix effects in the analysis of light elements in silicate minerals: Comparison with SREF and EMPA data. American Mineralogist. 87: 1477-1485.
Peacock, S.M., Hervig, R.L., 1999. Boron isotopic composition of subduction-zone metamorphic rocks. Chemical Geology. 160: 281-290.
Pivec, E., Štemprok, M., Novál, J.K., and Lang, M. 1998. Tourmaline as a late-magmatic or postmagmatic mineral in granites of the Czech part of the Krušné hory – Erzgebirge batholith and its contact zone. Journal of the Czech Geological Society. 43 (1): 17-23.
Quirt, D.H. (2015): "Dravite" – what should it be called?? AREVA Resources Canada Inc., Internal Report, No. 15-CND-51-03, 11 p.

Quirt, D.H., Kotzer, T., and Kyser, K. 1991. Tourmaline, phosphate minerals, zircon, and pitchblende in the Athabasca Group: Maw Zone and McArthur River areas, Saskatchewan. In: Summary of Investigations 1991, Saskatchewan Geological Survey, Saskatchewan Energy and Mines, Miscellaneous Report 91-4, p. 181-191.

Ramaekers, P., Jefferson, C.W., Yeo, G.M., Collier, B., Long, D.G.F., Drever, G., McHardy, S., Jiricka, D., Cutts, C., Wheatley, K., Catuneanu, O., Bernier, S., Kupsch, B., and Post, R.T., 2007, Revised geological map and stratigraphy of the Athabasca Group, Saskatchewan and Alberta, *in* Jefferson, C.W. and Delaney, G., eds., EXTECH IV: Geology and uranium exploration technology of the Proterozoic Athabasca Basin, Saskatchewan and Alberta, Geological Survey of Canada, Bulletin 588, p. 155-191.

Reid, K.D., Ansdell, K., Jiricka, D., Witt, G., and Card, C. 2013. Regional setting, geology, and paragenesis of the centennial unconformity-related uranium deposit, Athabasca Basin, Saskatchewan, Canada. Economic Geology. 109(3): 539-566.

Riciputi, L.R., Chacko, T., Cole, D.R., and Horita, J. 1997. Analysis of hydrogen isotope ratios by SIMS, and application to determining mineral-fluid isotope fractionation factors. In: G. Gillen, R.Lareau, J. Bennett, and F. Stevie, eds., SIMS XI proceedings, Wiley, Chichester, U.K., : 79-82.

Riciputi, L.R., Paterson, B.A., Ripperdan, R.L., 1998. Measurement of light stable isotope ratios by SIMS: Matrix effects for oxygen, carbon, and sulfur isotopes in minerals. International Journal of Mass Spectrometry. 178: 81-112.

Richard, A., Boulvais, P., Mercadier, J., Boiron, M-C., Cathelineau, M., Cuney, M., France-Lanord, C. 2013. From evaporated seawater to uranium-mineralizing brines: Isotopic and trace element study of quartz-dolomite veins in the Athabasca system. Geochimica et Cosmochimica Acta. 113: 38-59.

Rollion-Bard, C. and Marin-Carbonne, J., 2011. Determination of SIMS matrix effects on oxygen isotopic compositions in carbonates. Journal of Analytical Atomic Spectrometry. 26: 1285-1289.

Schmitt, A.K., and Zack, T. 2012. High-sensitivity U-Pb rutile dating by secondary ion mass spectrometry (SIMS) with an O_2^+ primary beam. Chemical Geology.332: 65-73.

Shabaga, B.M., Fayek, M., and Hawthorne, F.C. 2010. Boron and lithium isotopic compositions as provenance indicators of Cu-bearing tourmalines. Mineralogical Magazine. 74(2): 241-255.

Sharp, Z. 1990. A laser-based microanalytical method for the *in situ* determination of oxygen isotope ratios of silicates and oxides. Geochimical et Cosmochimica Acta. 54 (5): 1353-1357.

Sharp, Z. 2007. Principles of Stable Isotope Geochemistry. (ed. C. Rapp) Pearson Prentice Hall. Upper Saddle River, New Jersey.

Sheahan, C., Fayek, M., Quirt, D., and Jefferson, C.W. 2014. A combined ingress-egress model for the Kianna unconformity-related uranium deposit, Shea Creek Project, Athabasca Basin, Canada. Economic Geology. 111(1): 225-257.

Shuschevskaya, T., Ignatiev, A., and Velivtskaya, T. 2011. Magmatic nature of mineralizing fluids in the Solnechonoye Sn deposit (Russia) deduced from isotopic (H, O) compositions of- tourmaline. Resource Geology. 61(4): 407-413.

Taylor, R., Clark, C., and Reddy S.M., 2012. The effect of grain orientation on secondary ion mass spectrometry (SIMS) analysis of rutile. Chemical Geology. 300:81-87.

Tindle, A.G., Breaks, F.W., and Selway, J.B. 2002. Tourmaline in petalite-subtype granitic pegmatites: Evidence of fractionation and contamination from the Pakeagama Lake and

Separation Lake areas of northwestern Ontario, Canada. The Canadian Mineralogist. 40:753-788.
Tourigny, G., Quirt, D. H., Wilson, N.S.F., Wilson, S., Breton, G., and Portella, P. 2007. Geological and structural feautres of the Sue C uranium deposit, McClean Lake area, Saskatchewan. *in* Jefferson, C.W. and Delaney, G., eds., EXTECH IV: Geology and uranium exploration technology of the Proterozoic Athabasca Basin, Saskatchewan and Alberta, Geological Survey of Canada, Bulletin 588: 229-248.
Trumbull, R.B., and Chaussidon, M. 1999. Chemical and boron isotopic composition of magmatic and hydrothermal tourmalines form the Sinceni granite-pegmatite system in Swaziland. Chemical Geology. 153: 125-137.
Trumbull, R.B., Slack, J.F., Krienitz, M-S., Belkin, H.E., and Wiedenbeck, M. 2011. Fluid sources and metallogensis in the Blackbird Co-Cu-Au-Bi-REE district, Idaho, USA.: Insights from major-element and boron isotopic compositions of tourmaline. Canadian Mineralogist. 49: 225-244.
Valley, J.W., and Kita, N.T., 2009. *In Situ* oxygen isotope geochemistry by ion microprobe. In: Fayek, M. Ed. Secondary Ion Mass Spectrometry in the Earth Sciences: Gleaning the Big Picture from a Small Spot. Mineralogical Association of Canada Short Course Series Vol 41. Mineralogical Association of Canada, Québec, Québec.
Vennemann, T.W., and O'Neil, J.R., 1993. A simple inexpensive method of hydrogen isotope and water analyses of minerals and rocks based on zinc reagent. Chemical Geology. 103: 227-234.
Wingate, M.T.D., and Compston, W. 2000. Crystal orientation effects during ion microprobe U-Pb analysis of baddeleyite. Chemcial Geology. 168: 75-97.
Winter. J.D. 2010. An introduction to igneous and metamorphic petrology. (ed.N. Folchetti). Pearson Prentice Hall. Upper Saddle River, New Jersey.
Zachariáš, J., Žáček. V., Pudilová, M., and Machovič, V. 2005. Fluid inclusions and stable isotope study of quartz-tourmaline veins associated with beryl and emerald mineralization, Kafubu area, Zambia. Chemical Geology. 223: 136-152.
Zheng, Y.F. 1993. Calculation of oxygen isotope fractionation in hydroxy-bearing silicates. Earth and Planetary Science Letters. 120: 247-263.

Appendices

Appendix A: Electron Microprobe Standards and Data.

Table A.1 Elements analyzed by EMP and the standards used

Element	Standard
F	1-17 F-Riebeckite
Na	2-42 Albite
Mg	2-41 Olivine
Al	1-17 Adalusite
Si	2-29 Diopside
K	2-31 Orthoclase
Ca	2-29 Diopside
Ti	2-21 Sphene
Mn	2-20 Spessartine
Fe	1-14 Fayalite

Table A.2 - EMPA Data for Calibration Samples

Sample No.	Na_2O	SiO_2	CaO	FeO	MnO	Al_2O_3	F	MgO	K_2O	TiO_2	Total
BT -01	2.75	34.00	0.01	19.29	0.14	30.23	1.74	0.00	0.06	0.04	88.26
BT -01	2.77	33.99	0.04	18.94	0.11	30.88	2.01	0.01	0.05	0.03	88.83
BT -01	2.49	34.55	0.02	18.45	0.11	31.16	1.46	0.05	0.05	0.18	88.52
BT -01	2.55	34.61	0.00	17.82	0.07	31.52	1.65	0.03	0.05	0.16	88.46
BT -01	2.69	34.37	0.03	18.29	0.06	30.45	1.75	0.40	0.07	0.61	88.72
BT -01	2.75	34.08	0.03	19.33	0.06	30.03	2.00	0.18	0.05	0.31	88.82
BT -01	2.77	34.22	0.01	18.51	0.15	30.96	2.05	0.03	0.05	0.06	88.81
CE-01	2.07	39.22	0.00	0.03	0.06	43.40	0.87	0.00	0.02	0.00	85.67
CE-01	2.03	39.00	0.02	0.02	0.06	43.43	0.84	0.00	0.01	0.00	85.41
CE-01	2.03	39.10	0.00	0.02	0.04	43.49	0.84	0.00	0.01	0.00	85.53
CE-01	1.95	39.11	0.01	0.00	0.07	43.22	0.79	0.00	0.02	0.00	85.17
CE-01	2.01	39.00	0.00	0.00	0.06	43.60	0.84	0.00	0.01	0.00	85.52
PE-01	2.01	38.37	0.15	0.08	0.28	41.78	1.30	0.00	0.02	0.00	83.99
PE-01	1.96	38.33	0.24	0.08	0.63	42.48	1.32	0.00	0.01	0.01	85.06
PE-01	2.04	38.02	0.08	0.09	0.34	42.20	1.28	0.01	0.02	0.00	84.08
PE-01	2.06	38.44	0.23	0.14	0.77	42.01	1.37	0.01	0.01	0.01	85.05
PE-01	2.05	38.50	0.22	0.08	0.66	42.16	1.47	0.00	0.01	0.00	85.15
PE-01	1.98	38.41	0.34	0.16	0.74	41.97	1.59	0.00	0.02	0.01	85.22
BT-02	1.45	36.26	0.32	11.34	0.74	34.49	0.28	1.83	0.03	0.42	87.16
BT-02	1.32	36.85	0.12	11.53	0.76	35.28	0.12	1.73	0.01	0.11	87.83
BT-02	1.27	36.78	0.13	11.35	0.74	35.10	0.12	1.74	0.02	0.10	87.35
BT-02	1.54	36.33	0.32	11.25	0.76	34.94	0.28	1.82	0.02	0.39	87.65
BT-02	1.50	36.41	0.32	11.38	0.74	35.00	0.34	1.86	0.02	0.40	87.97
PE-02	1.84	38.48	0.98	0.02	1.02	41.45	1.47	0.00	0.02	0.01	85.29
PE-02	1.91	38.60	0.89	0.02	1.04	41.86	1.52	0.00	0.01	0.01	85.86
PE-02	1.89	38.78	0.89	0.01	1.11	42.02	1.72	0.01	0.01	0.00	86.44
PE-02	1.84	38.81	0.90	0.03	1.10	41.73	1.53	0.00	0.02	0.00	85.96
PE-02	1.87	38.68	0.90	0.02	1.20	41.74	1.59	0.00	0.01	0.00	86.01

Totals do not equal 100% as the EMPA does not account for B_2O_3, LiO_2 or H_2O

Table A.2 - EMPA Data for Calibration Samples

Sample No.	Na_2O	SiO_2	CaO	FeO	MnO	Al_2O_3	F	MgO	K_2O	TiO_2	Total
GE-01	2.09	38.21	2.00	0.03	0.00	29.97	1.19	13.14	0.01	0.98	87.62
GE-01	1.67	38.11	2.74	0.03	0.00	29.51	1.22	13.35	0.01	0.90	87.54
GE-01	1.52	38.07	3.04	0.03	0.00	28.97	1.44	14.00	0.00	0.85	87.92
GE-01	2.32	38.43	1.50	0.03	0.01	31.18	0.72	12.58	0.01	0.62	87.40
GE-02	1.08	37.77	3.81	0.05	0.00	27.89	1.65	14.32	0.01	1.19	87.77
GE-02	1.01	37.87	3.97	0.07	0.02	27.93	1.48	14.27	0.00	1.30	87.92
GE-02	0.98	37.71	3.99	0.03	0.00	27.98	1.72	14.27	0.00	1.22	87.90
GE-02	1.06	37.69	3.95	0.03	0.01	27.91	1.57	14.17	0.01	1.18	87.58
GE-02	1.36	38.10	3.29	0.04	0.02	28.87	1.58	13.96	0.02	0.86	88.10
DRG	2.24	37.43	0.73	4.93	0.02	33.11	1.03	8.57	0.01	0.31	88.38
DRG	2.39	37.34	0.74	5.01	0.02	33.08	0.89	8.51	0.01	0.32	88.31
DRG	2.36	37.60	0.61	4.67	0.01	33.52	0.96	8.45	0.02	0.28	88.48

Totals do not equal 100% as the EMPA does not account for B_2O_3, LiO_2 or H_2O

Table A.3 EMPA Data for Application Samples

Sample No.	Na_2O	SiO_2	CaO	FeO	MnO	Al_2O_3	F	MgO	K_2O	TiO_2	Total
R237-DR6	2.03	33.64	0.34	10.36	0.03	33.75	0.27	3.18	0.05	1.11	84.76
R237-DR6	1.84	33.82	0.40	11.09	0.10	34.49	0.12	2.68	0.04	1.17	85.75
R237-DR6	2.11	35.09	0.42	10.44	0.05	34.52	0.31	3.40	0.05	1.03	87.42
R237-DR6	1.84	35.11	0.72	9.34	0.03	34.20	0.36	4.46	0.06	1.18	87.30
R237-DR6	1.38	34.46	0.80	8.53	0.08	32.84	0.22	4.52	0.07	1.01	83.91
R237-DR6	1.98	35.64	0.49	9.17	0.00	34.42	0.28	4.55	0.05	0.89	87.47
R237-DR7	2.11	34.25	0.38	9.01	0.01	33.68	0.31	4.35	0.04	1.12	85.26
R237-DR7	2.07	34.23	0.55	9.38	0.07	33.80	0.39	4.41	0.08	0.99	85.97
R237-DR7	2.02	34.66	0.51	9.23	0.00	34.06	0.31	4.44	0.06	1.03	86.32
R237-DR7	1.97	33.80	0.43	10.40	0.06	34.67	0.14	3.08	0.04	1.15	85.74
R237-DR7	1.92	33.52	0.23	10.58	0.01	34.34	0.09	2.68	0.12	0.54	84.03
R237-DR7	1.82	35.16	0.18	10.45	0.00	35.33	0.20	2.66	0.03	0.53	86.36
R237-DR7	1.93	32.60	0.65	9.04	0.05	32.42	0.38	4.54	0.06	1.10	82.77
R237-DR8	1.94	34.87	0.63	8.92	0.02	33.64	0.30	4.83	0.06	1.03	86.24
R237-DR8	2.13	35.23	0.25	9.70	0.04	34.95	0.22	4.02	0.03	0.97	87.54
R237-DR8	2.05	34.09	0.36	9.19	0.00	34.46	0.25	4.21	0.03	0.76	85.40
R237-DR8	1.99	34.39	0.57	9.18	0.03	33.97	0.21	4.47	0.04	0.96	85.81
R237-DR8	2.06	35.01	0.65	8.74	0.02	33.70	0.00	4.83	0.06	1.06	86.13
R237-DR8	2.01	34.46	0.49	9.47	0.05	33.69	0.27	4.26	0.05	1.01	85.76
SL81TL-DR4	1.97	35.82	1.08	6.52	0.01	33.82	0.29	3.68	0.06	1.26	84.51
SL81TL-DR4	1.83	36.11	1.14	6.46	0.00	33.94	0.47	6.56	0.05	1.36	87.92
SL81TL-DR4	1.76	35.59	1.34	6.31	0.00	33.10	0.32	6.92	0.07	1.71	87.12
SL81TL-DR4	1.78	35.88	1.39	6.47	0.01	33.70	0.29	6.92	0.09	1.43	87.96
SL81TL-DR4	1.79	35.59	1.35	6.45	0.01	33.07	0.19	6.62	0.08	1.37	86.52
SL81TL-DR4	1.75	35.62	1.32	6.26	0.06	33.14	0.21	6.90	0.08	1.50	86.84
SL81TL-DR5	1.91	35.32	1.09	6.37	0.00	33.38	0.32	6.62	0.08	1.22	86.31
SL81TL-DR5	1.83	35.66	1.41	6.52	0.05	32.96	0.39	6.85	0.07	1.42	87.16
SL81TL-DR5	1.94	35.61	1.14	6.42	0.00	33.51	0.45	6.56	0.06	1.26	86.95
SL81TL-DR5	1.90	35.68	1.09	6.37	0.02	33.84	0.27	6.45	0.06	1.32	87.00

Totals do not equal 100% as the EMPA does not account for B_2O_3, LiO_2 or H_2O

Table A.3 EMPA Data for Application Samples

Sample No	Na_2O	SiO_2	CaO	FeO	MnO	Al_2O_3	F	MgO	K_2O	TiO_2	Total
SL81TL-DR6	1.97	35.53	1.24	6.38	0.00	33.50	0.31	6.70	0.08	1.36	87.06
SL81TL-DR6	1.85	35.61	1.15	7.35	0.05	33.83	0.33	5.89	0.10	1.28	87.44
SL81TL-DR6	1.77	35.65	1.31	6.57	0.01	33.45	0.52	6.76	0.07	1.38	87.49
SL81TL-DR6	1.81	35.68	1.16	6.48	0.01	33.82	0.35	6.58	0.09	1.34	87.32
SL81TL-DR6	1.84	35.44	1.16	6.50	0.03	33.49	0.40	6.68	0.08	1.34	86.96
SL81TL-DR6	1.94	35.94	0.54	8.34	0.03	34.69	0.19	4.83	0.06	1.02	87.57
SL81TL-DR7	1.51	35.74	0.70	6.21	0.01	33.08	0.17	6.56	0.06	0.69	84.74
SL81TL-DR7	1.86	36.00	1.34	6.40	0.03	33.08	0.37	6.97	0.07	1.38	87.50
SL81TL-DR7	1.80	35.40	1.38	6.35	0.03	32.81	0.35	6.79	0.06	1.43	86.41
SL81TL-DR7	1.67	35.76	1.37	6.55	0.00	33.36	0.17	6.67	0.06	1.38	87.00
SL81TL-DR7	1.75	35.52	1.35	6.52	0.01	33.07	0.44	6.73	0.07	1.42	86.88
SL81TL-DR8	1.92	35.45	0.63	6.94	0.01	34.39	0.31	5.71	0.08	1.19	86.61
SL81TL-DR8	1.95	35.85	1.30	6.42	0.01	33.42	0.35	6.83	0.09	1.39	87.61
SL81TL-DR8	1.70	35.62	1.35	7.02	0.03	33.50	0.22	6.38	0.07	1.39	87.29
SL81TL-DR8	1.77	35.74	1.31	6.41	0.00	33.36	0.42	6.78	0.09	1.42	87.30
SL81TL-DR9	1.69	35.75	1.10	6.44	0.00	33.73	0.29	6.47	0.08	1.15	86.71
SL81TL-DR9	1.84	36.03	0.99	6.32	0.03	33.68	0.41	6.39	0.08	1.24	87.01
SL81TL-DR9	1.82	35.71	0.99	6.51	0.03	33.46	0.51	6.71	0.06	1.19	86.99
SL81TL-DR9	1.77	35.35	1.11	6.36	0.05	33.34	0.30	6.63	0.07	1.40	86.38
SL81TL-DR9	1.79	35.52	1.31	6.34	0.00	33.19	0.53	7.00	0.07	1.38	87.14
SL81-DR11	1.86	34.70	0.62	8.58	0.02	33.87	0.18	4.64	0.07	1.15	85.69
SL81-DR11	1.79	35.80	1.26	6.33	0.00	33.15	0.30	6.69	0.09	1.44	86.85
SL81-DR11	1.85	35.80	1.33	6.37	0.00	33.30	0.43	6.84	0.09	1.46	87.47
SL81-DR11	1.68	35.83	1.34	6.40	0.00	33.16	0.53	6.94	0.08	1.45	87.41
SL81TL-DR12	1.67	35.75	1.07	6.49	0.04	33.56	0.28	6.56	0.07	1.31	86.80
SL81TL-DR12	1.76	36.36	1.30	6.34	0.01	33.49	0.40	6.87	0.08	1.38	87.99
SL81TL-DR12	1.74	35.44	1.24	6.40	0.01	33.25	0.35	6.70	0.08	1.37	86.57
SL81TL-DR12	1.84	35.65	1.10	6.26	0.00	32.87	0.29	6.57	0.08	1.49	86.15

Totals do not equal 100% as the EMPA does not account for B_2O_3, LiO_2 or H_2O

Table A.3 EMPA Data for Application Samples

Sample No	Na_2O	SiO_2	CaO	FeO	MnO	Al_2O_3	F	MgO	K_2O	TiO_2	Total
SL81TL-DR13	1.64	35.34	1.33	6.71	0.03	33.20	0.40	6.47	0.09	1.33	86.54
SL81TL-DR13	1.96	35.29	0.63	7.38	0.00	34.47	0.46	5.47	0.06	1.16	86.87
SL81TL-DR13	1.70	35.56	1.23	6.45	0.01	33.56	0.27	6.63	0.06	1.34	86.81
SL81TL-DR13	1.70	35.53	1.28	6.49	0.01	33.28	0.18	6.46	0.08	1.37	86.38
SL81TL-DR13	1.85	33.02	1.14	6.50	0.00	32.48	0.56	6.38	0.07	1.28	83.28
SL81BR	1.83	35.90	1.26	6.30	0.02	33.53	0.39	6.79	0.07	1.36	87.47
SL81BR	1.83	36.22	1.16	6.38	0.03	33.69	0.38	6.71	0.09	1.31	87.78
SL81BR	1.92	35.54	1.12	6.46	0.02	33.91	0.43	6.53	0.08	1.28	87.29
SL81BR	1.69	35.38	1.32	6.62	0.01	33.43	0.44	6.59	0.08	1.39	86.96
SL81BR	1.85	34.60	1.15	6.35	0.03	33.08	0.33	6.45	0.06	1.34	85.22

Totals do not equal 100% as the EMPA does not account for B_2O_3, LiO_2 or H_2O

Appendix B
LA-ICP-MS Data for Calibration Samples

Table B.1 LA-ICP-MS Data for Li and B concentrations of Calibration samples

Sample No	Li_2O	B_2O_3	Sample No	Li_2O	B_2O_3
BT-01	0.09	10.88	GE-01	0.00	11.11
BT-01	0.07	10.94	GE-01	bdl	11.35
BT-01	0.07	11.08	GE-01	bdl	11.34
BT-01	0.08	10.90	GE-01	0.00	11.34
BT-01	0.09	11.02	GE-01	0.00	11.19
BT-01	0.05	11.03	GE-02	0.00	11.24
BT-02	0.07	11.02	GE-02	bdl	11.23
BT-02	0.07	10.93	GE-02	bdl	11.17
BT-02	0.15	11.32	GE-02	bdl	11.30
BT-02	0.11	10.97	GE-02	0.00	11.01
BT-02	0.07	10.76	PE-01	2.74	11.78
CE-01	0.07	12.73	PE-01	2.21	12.11
CE-01	0.05	13.20	PE-01	1.90	13.27
CE-01	0.08	12.84	PE-01	2.70	12.09
CE-01	0.07	13.67	PE-01	2.28	13.14
CE-01	0.07	12.38	PE-02	2.37	11.06
CE-01	0.06	13.56	PE-02	2.45	11.00
DRG	0.00	11.12	PE-02	2.41	11.25
DRG	0.00	11.05	PE-02	2.43	11.38
DRG	0.00	10.96	PE-02	2.37	11.10
DRG	0.00	11.16			
DRG	0.00	11.14			

bdl= below detection limit

Appendix C
SIMS Data for Calibration Samples

Table C.1: SIMS analyses of calibration samples for oxygen isotope ratios

December 1, 2014 Sample	$^{18}O/^{16}O$	1σ	FF	Mass Bias
PE-01	1.885791	1.2	0.9290	-71.0
PE-01	1.888788	1.2	0.9305	-69.5
PE-01	1.889285	1.2	0.9307	-69.3
PE-01	1.888275	1.2	0.9302	-69.8
Average	1.888035		0.9301	-69.9
St Deviation	0.0013		0.0007	0.7
True Value	2.029864			
BT-02	1.895838	1.2	0.9391	-60.9
BT-02	1.896611	1.1	0.9395	-60.5
BT-02	1.896288	1.2	0.9393	-60.7
BT-02	1.894155	1.2	0.9382	-61.8
BT-02	1.894128	1.2	0.9382	-61.8
Average	1.895404		0.9389	-61.1
St Deviation	0.0011		0.0005	0.5
True Value	2.018835			
PE-02	1.885382	1.2	0.9302	-69.8
PE-02	1.887435	1.2	0.9312	-68.8
PE-02	1.885332	1.2	0.9302	-69.8
PE-02	1.889512	1.2	0.9322	-67.8
Average	1.886915		0.9310	-69.0
St Deviation	0.0017		0.0008	0.8
True Value	2.026856			
GE-01	1.904821	1.2	0.9316	-68.4
GE-01	1.908916	1.2	0.9336	-66.4
GE-01	1.902138	1.2	0.9303	-69.7
GE-01	1.905385	1.2	0.9319	-68.1
Average	1.905315		0.9318	-68.2
St Deviation	0.0024		0.0012	1.2
True Value	2.044702			
GE-02	1.901096	1.2	0.9298	-70.2
GE-02	1.905244	1.2	0.9318	-68.2
GE-02	1.902310	1.1	0.9304	-69.6
GE-02	1.910321	1.2	0.9343	-65.7
Average	1.904743		0.9316	-68.4
St Deviation	0.0036		0.0017	1.7
True Value	2.044702			

Table C.1: SIMS analyses of calibration samples for oxygen isotope ratios

December 2, 2014 Sample	$^{18}O/^{16}O$	1σ	FF	Mass Bias
DRG	1.897239	1.2	0.9336	-66.4
DRG	1.898149	1.2	0.9341	-65.9
DRG	1.895364	1.2	0.9327	-67.3
DRG	1.898218	1.2	0.9341	-65.9
Average	1.897243		0.9337	-66.3
St Deviation	0.0012		0.0006	0.6
True Value	2.032070			
Decemeber 4, 2014				
BT-01	1.912932	2.2	0.9450	-55.0
BT-01	1.913579	1.2	0.9453	-54.7
BT-01	1.915470	1.2	0.9463	-53.7
BT-01	1.915451	1.2	0.9463	-53.7
Average	1.914358		0.9457	-54.3
St Deviation	0.0011		0.0006	0.6
True Value	2.024249			
CE-01	1.893951	1.2	0.9314	-68.6
CE-01	1.890665	1.2	0.9298	-70.2
CE-01	1.891794	1.2	0.9303	-69.7
CE-01	1.893121	1.2	0.9310	-69.0
Average	1.892383		0.9306	-69.4
St Deviation	0.0013		0.0006	0.6
True Value	2.033473			

Table C.2: SIMS analyses of calibration samples for hydrogen isotope ratios

June 10, 2015 Sample	D/H	1σ	FF	Mass Bias
BT-01	5.314580E-05	12.0	0.3741	-626
BT-01	5.393831E-05	12.0	0.3797	-620
BT-01	5.435422E-05	12.0	0.3826	-617
BT-01	5.364645E-05	13.0	0.3777	-622
BT-01	5.356087E-05	12.0	0.3770	-623
BT-01	5.356149E-05	12.0	0.3771	-623
Average	5.370119E-05		0.3780	-622
St. Deviation	3.726782E-07		0.0026	3
True Value	1.420531E-03			
BT-02	4.808635E-05	11.0	0.3298	-670
BT-02	4.845280E-05	12.0	0.3323	-668
BT-02	4.818232E-05	11.0	0.3305	-670
BT-02	4.725106E-05	11.0	0.3241	-676
BT-02	4.788208E-05	11.0	0.3284	-672
BT-02	4.770659E-05	11.0	0.3272	-673
Average	4.792687E-05		0.3287	-671
St. Deviation	3.817808E-07		0.0026	3
True Value	1.457914E-03			
CE-01	4.993040E-05	12.0	0.3523	-648
CE-01	4.882487E-05	12.0	0.3445	-656
CE-01	4.895428E-05	12.0	0.3454	-655
CE-01	4.946254E-05	12.0	0.3490	-651
CE-01	4.946168E-05	12.0	0.3490	-651
CE-01	5.198142E-05	12.0	0.3667	-633
CE-01	5.045721E-05	12.0	0.3560	-644
Average	4.986749E-05		0.3518	-648
St. Deviation	1.004995E-06		0.0071	7
True Value	1.403398E-03			
DRG	4.979789E-05	12.7	0.3316	-668
DRG	5.043856E-05	11.8	0.3359	-664
DRG	5.046708E-05	11.5	0.3361	-664
DRG	4.981474E-05	11.6	0.3318	-668
DRG	4.941964E-05	12.6	0.3291	-671
DRG	5.041428E-05	11.5	0.3358	-664
Average	5.005870E-05		0.3334	-667
St. Deviation	4.027905E-07		0.0027	3
True Value	1.484393E-03			

Table C.2: SIMS analyses of calibration samples for hydrogen isotope ratios

June 10, 2015 Sample	D/H	1σ	FF	Mass Bias
GE-01	5.031732E-05	12.0	0.3400	-660
GE-01	4.935114E-05	13.0	0.3335	-666
GE-01	5.092751E-05	12.0	0.3442	-656
GE-01	5.076701E-05	11.9	0.3431	-657
GE-01	5.077678E-05	12.0	0.3432	-657
GE-01	4.968357E-05	13.0	0.3358	-664
Average	5.030389E-05		0.3400	-660
St. Deviation	5.943788E-07		0.0040	4
True Value	1.479720E-03			
GE-02	5.032843E-05	12.9	0.3401	-660
GE-02	5.183578E-05	12.9	0.3503	-650
GE-02	5.154646E-05	17.6	0.3484	-652
GE-02	5.106744E-05	12.9	0.3451	-655
GE-02	5.007365E-05	12.9	0.3384	-662
GE-02	5.049918E-05	13.2	0.3413	-659
Average	5.089182E-05		0.3439	-656
St. Deviation	6.443903E-07		0.0044	4
True Value	1.479720E-03			
PE-01	4.807726E-05	13	0.3449	-655
PE-01	4.715742E-05	13	0.3383	-662
PE-01	4.805604E-05	13	0.3447	-655
PE-01	4.825592E-05	13	0.3462	-654
PE-01	4.730294E-05	13	0.3393	-661
PE-01	4.703367E-05	13	0.3374	-663
Average	4.764721E-05		0.3418	-658
St. Deviation	4.928590E-07		0.0035	4
True Value	1.394052E-03			
PE-02	4.96544E-05	12	0.3476	-652
PE-02	5.02834E-05	13	0.3520	-648
PE-02	4.98827E-05	12	0.3492	-651
PE-02	5.01197E-05	12	0.3509	-649
PE-02	5.05362E-05	12	0.3538	-646
PE-02	5.14542E-05	13	0.3602	-640
Average	5.032175E-05		0.3523	-648
St. Deviation	5.786233E-07		0.0041	4
True Value	1.428319E-03			

Table C.3: SIMS analyses of oxygen isotopes for crystallographically oriented samples

August 26, 2015 Sample	Orientation	$^{18}O/^{16}O$	1σ	FF	Mass Bias
BT-01	∥ c-axis	1.920710	1.2	0.9489	-51.1
BT-01	∥ c-axis	1.918807	1.2	0.9479	-52.1
BT-01	∥ c-axis	1.918524	1.2	0.9478	-52.2
BT-01	∥ c-axis	1.920638	1.2	0.9488	-51.2
BT-01	∥ c-axis	1.918397	1.2	0.9477	-52.3
Average		1.919415		0.9482	-51.8
St. Deviation		0.001037		0.0005	0.5
True Value	2.024249				
BT-01	⊥ c axis	1.919423	1.2	0.9482	-51.8
BT-01	⊥ c axis	1.920925	1.2	0.9490	-51.0
BT-01	⊥ c axis	1.921994	1.2	0.9495	-50.5
BT-01	⊥ c axis	1.922546	1.2	0.9498	-50.2
BT-01	⊥ c axis	1.916914	2.2	0.9470	-53.0
BT-01	⊥ c axis	1.920680	1.2	0.9489	-51.1
Average		1.920414		0.9487	-51.3
St. Deviation		0.001853		0.0009	0.9
True Value	2.024249				
PE-01	∥ c-axis	1.896598	1.2	0.9343	-65.7
PE-01	∥ c-axis	1.896881	1.2	0.9345	-65.5
PE-01	∥ c-axis	1.896732	1.2	0.9344	-65.6
PE-01	∥ c-axis	1.901112	1.2	0.9366	-63.4
PE-01	∥ c-axis	1.900098	1.2	0.9361	-63.9
PE-01	∥ c-axis	1.892490	1.2	0.9323	-67.7
Average		1.897319		0.9347	-65.3
St. Deviation		0.002783		0.0014	1.4
True Value	2.029864				
PE-01	⊥ c axis	1.900597	1.2	0.9363	-63.7
PE-01	⊥ c axis	1.895719	1.2	0.9339	-66.1
PE-01	⊥ c axis	1.899486	1.2	0.9358	-64.2
PE-01	⊥ c axis	1.896993	1.2	0.9345	-65.5
PE-01	⊥ c axis	1.900023	1.2	0.9360	-64.0
PE-01	⊥ c axis	1.898054	1.2	0.9350	-65.0
Average		1.898479		0.9353	-64.7
St. Deviation		0.001727		0.0009	0.9
True Value	2.029864				

Table C.3: SIMS analyses of oxygen isotopes for crystallographically oriented samples

August 26, 2015 Sample	Orientation	$^{18}O/^{16}O$	1σ	FF	Mass Bias
PE-02	∥ c-axis	1.892697	1.2	0.9338	-66.2
PE-02	∥ c-axis	1.894234	1.2	0.9345	-65.5
PE-02	∥ c-axis	1.889539	1.2	0.9322	-67.8
PE-02	∥ c-axis	1.892035	1.2	0.9335	-66.5
PE-02	∥ c-axis	1.896091	2.2	0.9355	-64.5
PE-02	∥ c-axis	1.891008	1.2	0.9330	-67.0
Average		1.892601		0.9337	-66.3
St. Deviation		0.002125		0.0010	1.0
True Value	2.026856				
PE-02	⊥ c axis	1.898755	1.2	0.9368	-63.2
PE-02	⊥ c axis	1.892607	1.2	0.9337	-66.3
PE-02	⊥ c axis	1.894754	1.2	0.9348	-65.2
PE-02	⊥ c axis	1.893975	1.2	0.9344	-65.6
PE-02	⊥ c axis	1.889779	2.2	0.9323	-67.7
PE-02	⊥ c axis	1.890487	1.2	0.9327	-67.3
Average		1.893393		0.9341	-65.9
St. Deviation		0.002974		0.0015	1.5
True Value	2.026856				

Table C.4: SIMS analyses of hydrogen isotopes for crystallographically oriented samples

August 31, 2015 Sample	Orientation	D/H	1σ	FF	Mass Bias
BT-01	∥ c-axis	4.536770E-05	13.4	0.3194	-681
BT-01	∥ c-axis	4.468486E-05	13.3	0.3146	-685
BT-01	∥ c-axis	4.438437E-05	14.3	0.3124	-688
BT-01	∥ c-axis	4.555221E-05	13.2	0.3207	-679
BT-01	∥ c-axis	4.607856E-05	13.0	0.3244	-676
BT-01	∥ c-axis	4.636389E-05	13.0	0.3264	-674
Average		4.540527E-05		0.3196	-680
St. Deviation		7.019618E-07		0.0049	5
True Value	1.420531E-04				
BT-01	⊥ c axis	4.704314E-05	12.8	0.3312	-669
BT-01	⊥ c axis	4.752011E-05	12.7	0.3345	-665
BT-01	⊥ c axis	4.835521E-05	12.7	0.3404	-660
BT-01	⊥ c axis	4.619691E-05	13.7	0.3252	-675
BT-01	⊥ c axis	4.770110E-05	12.7	0.3358	-664
BT-01	⊥ c axis	4.774703E-05	12.9	0.3361	-664
Average		4.742725E-05		0.3339	-666
St. Deviation		6.718458E-07		0.0047	4
True Value	1.420531E-04				
PE-01	∥ c-axis	3.968711E-05	14.1	0.2847	-715
PE-01	∥ c-axis	3.888299E-05	14.1	0.2789	-721
PE-01	∥ c-axis	4.013231E-05	14.3	0.2879	-712
PE-01	∥ c-axis	4.058224E-05	13.9	0.2911	-709
PE-01	∥ c-axis	3.997581E-05	13.9	0.2868	-713
PE-01	∥ c-axis	3.997677E-05	13.8	0.2868	-713
Average		3.987287E-05		0.2860	-714
St. Deviation		5.174096E-07		0.0037	3
True Value	1.394052E-04				

∥ c-axis: parallel to the c-axis of the grain

⊥ c axis: perpendicular to the c-axis of the grain

Table C.4: SIMS analyses of hydrogen isotopes for crystallographically oriented samples

August 31, 2015 Sample	Orientation	D/H	1σ	FF	Mass Bias
PE-01	⊥ c axis	4.205488E-05	12.8	0.3017	-698
PE-01	⊥ c axis	4.170912E-05	13.1	0.2992	-701
PE-01	⊥ c axis	4.255956E-05	12.9	0.3053	-695
PE-01	⊥ c axis	4.160602E-05	13.1	0.2985	-702
PE-01	⊥ c axis	4.157179E-05	12.9	0.2982	-702
PE-01	⊥ c axis	4.221466E-05	12.6	0.3028	-697
Average		4.195267E-05		0.3009	-699
St. Deviation		3.586906E-07		0.0026	2
True Value	1.394052E-04				
PE-02	∥ c-axis	4.448077E-05	13.4	0.3114	-689
PE-02	∥ c-axis	4.321748E-05	13.2	0.3026	-697
PE-02	∥ c-axis	4.393534E-05	13.4	0.3076	-692
PE-02	∥ c-axis	4.492624E-05	14.4	0.3145	-685
PE-02	∥ c-axis	4.355798E-05	13.4	0.3050	-695
PE-02	∥ c-axis	4.348469E-05	13.5	0.3044	-696
Average		4.393375E-05		0.3076	-692
St. Deviation		5.972396E-07		0.0042	4
True Value	1.428319E-04				
PE-02	⊥ c axis	4.385653E-05	13.2	0.3070	-693
PE-02	⊥ c axis	4.456958E-05	13.2	0.3120	-688
PE-02	⊥ c axis	4.168813E-05	14.2	0.2919	-708
PE-02	⊥ c axis	4.127065E-05	15.2	0.2889	-711
PE-02	⊥ c axis	4.303106E-05	13.5	0.3013	-699
PE-02	⊥ c axis	4.300858E-05	13.2	0.3011	-699
Average		4.290409E-05		0.3004	-700
St. Deviation		1.144168E-06		0.0080	7
True Value	1.428319E-04				

∥ c-axis: parallel to the c-axis of the grain

⊥ c axis: perpendicular to the c-axis of the grain

Table C.4: SIMS analyses of hydrogen isotopes for crystallographically oriented samples

November 18, 2015 Sample	Orientation	D/H	1σ	FF	Mass Bias
BT-01	∥ c-axis	5.453590E-05	13.4	0.3839	-616
BT-01	∥ c-axis	5.437114E-05	13.3	0.3828	-617
BT-01	∥ c-axis	5.487311E-05	13.4	0.3863	-614
BT-01	∥ c-axis	5.567948E-05	13.2	0.3920	-608
BT-01	∥ c-axis	5.508553E-05	13.6	0.3878	-612
BT-01	∥ c-axis	5.371210E-05	13.5	0.3781	-622
Average		5.470954E-05		0.3851	-615
St. Deviation		6.121627E-07		0.0043	4
True Value	0.000142				
BT-01	⊥ c axis	5.630571E-05	12.7	0.3964	-604
BT-01	⊥ c axis	5.762388E-05	13.7	0.4057	-594
BT-01	⊥ c axis	5.621934E-05	12.6	0.3958	-604
BT-01	⊥ c axis	5.655501E-05	12.8	0.3981	-602
BT-01	⊥ c axis	5.638813E-05	12.7	0.3970	-603
BT-01	⊥ c axis	5.684002E-05	12.9	0.4001	-600
Average		5.665535E-05		0.3988	-601
St. Deviation		4.771409E-07		0.0034	3
True Value	0.000142				
CE-01	∥ c-axis	5.184388E-05	11.8	0.3694	-631
CE-01	∥ c-axis	5.017681E-05	11.9	0.3575	-642
CE-01	∥ c-axis	5.321134E-05	11.9	0.3792	-621
CE-01	∥ c-axis	5.179316E-05	12.1	0.3691	-631
CE-01	∥ c-axis	5.175963E-05	11.8	0.3688	-631
CE-01	∥ c-axis	5.038312E-05	12.0	0.3590	-641
Average		5.152799E-05		0.3672	-633
St. Deviation		1.016025E-06		0.0072	7
True Value	0.0001403				
CE-01	⊥ c axis	5.214870E-05	12.0	0.3716	-628
CE-01	⊥ c axis	5.056656E-05	12.0	0.3603	-640
CE-01	⊥ c axis	5.086876E-05	12.0	0.3625	-638
CE-01	⊥ c axis	5.124374E-05	12.0	0.3651	-635
CE-01	⊥ c axis	5.029573E-05	12.0	0.3584	-642
Average		5.102470E-05		0.3636	-636
St. Deviation		6.445093E-07		0.0046	5
True Value	0.0001403				

∥ c-axis: parallel to the c-axis of the grain

⊥ c axis: perpendicular to the c-axis of the grain

Table C.4: SIMS analyses of hydrogen isotopes for crystallographically oriented samples

November 18, 2015 Sample	Orientation	D/H	1σ	FF	Mass Bias
PE-01	∥ c-axis	4.858534E-05	12.0	0.3485	-651
PE-01	∥ c-axis	4.754542E-05	12.1	0.3411	-659
PE-01	∥ c-axis	4.720453E-05	12.1	0.3386	-661
PE-01	∥ c-axis	4.793721E-05	12.2	0.3439	-656
PE-01	∥ c-axis	4.642301E-05	12.1	0.3330	-667
PE-01	∥ c-axis	4.634213E-05	12.2	0.3324	-668
Average		4.733961E-05		0.3396	-660
St. Deviation		7.963139E-07		0.0057	6
True Value	0.000139				
PE-01	⊥ c axis	5.134642E-05	12.7	0.3683	-632
PE-01	⊥ c axis	4.922684E-05	12.7	0.3531	-647
PE-01	⊥ c axis	4.905923E-05	12.7	0.3519	-648
PE-01	⊥ c axis	4.980192E-05	12.7	0.3572	-643
PE-01	⊥ c axis	4.848125E-05	12.8	0.3478	-652
PE-01	⊥ c axis	4.874990E-05	12.7	0.3497	-650
Average		4.944426E-05		0.3547	-645
St. Deviation		9.443849E-07		0.0068	7
True Value	0.000139				
PE-02	∥ c-axis	5.195354E-05	12.5	0.3727	-636
PE-02	∥ c-axis	5.038116E-05	12.6	0.3614	-647
PE-02	∥ c-axis	5.200567E-05	12.7	0.3731	-636
PE-02	∥ c-axis	5.166708E-05	12.8	0.3706	-638
PE-02	∥ c-axis	5.097972E-05	12.0	0.3657	-643
PE-02	∥ c-axis	5.134522E-05	12.3	0.3683	-641
Average		5.138873E-05		0.3686	-640
St. Deviation		5.717639E-07		0.0041	4
True Value	0.000143				
PE-02	⊥ c axis	5.198669E-05	12.1	0.3729	-636
PE-02	⊥ c axis	5.106808E-05	12.2	0.3663	-642
PE-02	⊥ c axis	5.244878E-05	12.3	0.3762	-633
PE-02	⊥ c axis	5.043827E-05	12.2	0.3618	-647
PE-02	⊥ c axis	5.132629E-05	12.4	0.3682	-641
PE-02	⊥ c axis	5.243970E-05	12.3	0.3762	-633
Average		5.161797E-05		0.3703	-639
St. Deviation		7.394354E-07		0.0053	5
True Value	0.000143				

∥ c-axis: parallel to the c-axis of the grain

⊥ c axis: perpendicular to the c-axis of the grain